OPTIMIZED SILICON SOLAR CELLS

FOR

SPACE EXPLORATION POWER SYSTEMS

FINAL REPORT

NOVEMBER 30, 1971

Prepared by Peter A. Iles

JPL Contract No. 952865

Centralab Semiconductor Division
Globe-Union Inc.

4501 North Arden Drive
El Monte, California 91734

OPTIMIZED SILICON SOLAR CELLS

FOR

SPACE EXPLORATION POWER SYSTEMS

FINAL REPORT

NOVEMBER 30, 1971

Prepared by Peter A. Iles

JPL Contract No. 952865

Centralab Semiconductor Division
Globe-Union Inc.

4501 North Arden Drive
El Monte, California 91734

A B S T R A C T

This report describes a program aimed at designing and fabricating improved silicon solar cells for a range of missions extending from 0.1 to 15 astronomical units (Mercury to Jupiter).

Theoretical analysis was combined with some previous empirical measurements to design cells for five specific planetary missions.

For missions lying inside Earth radius (Mercury, Venus) the major cell property required was very low series resistance, allowing high curve fill factor to be maintained at the higher intensities. For the Mercury mission, the temperature of the cell had to be kept low. This was achieved by reflecting more of the incident sunlight by use of large area front contacts.

Theoretical estimates showed no advantage in shifting the reflectivity minimum of the anti-reflection coating to longer wavelengths. Optimum grid patterns were derived and used.

For the outer missions (Mars, the Asteroid belts and Jupiter) the formation of a Schottky barrier at the back contact had to be avoided (by use of a P+ layer under the back contact) and the excess leakage current of the PN junction had to be reduced. This reduction involved adjustment of several fabrication parameters and was the most difficult to ensure. When these two problems were minimized, the CFF of the cells remained high for operation at the low temperatures and intensities. Optimum grid patterns were also derived and used for these missions.

A parallel approach was followed, wherein widely separated values of four cell variables were combined in a matrix arrangement, and the cells measured over the whole range of missions to see if some of the combinations showed promise for specific missions.

Following the theoretical analysis, eleven groups of cells were fabricated, at least two groups being specifically designed for each of the five target missions. Also, the sixteen matrix groups were fabricated. Later, seven groups of deliverable cells were fabricated, including at least one group intended for each target mission.

Testing and analysis of all groups was performed at 28°C. This testing included I-V curves at three different intensities (5, 140, 850 mW/cm), dark forward and reverse I-V characteristics, and spectral response measurements.

The planned measurements at simulated mission conditions have not yet been made, thus preventing final conclusions from being made. These measurements will be performed subsequent to this report, and the results will be reported separately.

TABLE OF CONTENTS

List of Tables

LIST OF FIGURES

GLOSSARY OF TERMS USED

The following terms are used frequently in solar cell work. The definitions generally accepted in this work are given below.

1. AMO (Air Mass Zero)
   Refers to the intensity of sunlight measured near to space conditions (very low air mass between the sun and the measurement point). The solar spectrum used with AMO sunlight is that published by Johnson (F. S. Johnson, "The Solar Constant" J. Meteorol, Vol. 11, p. 431, 1954).

2. Cell Parameters
   These are the physical properties of the silicon, the contacts or the coating. They are determined by the fabrication sequence used.

3. Curve Fill Factor (CFF)
   See item 7. below.

4. Diffusion
   Used in two senses. First, it describes the solid state process whereby impurities are introduced into the silicon, generally to form a layer of conductivity sign opposite to that of the starting silicon. Second, it describes the motion of current carriers without the presence of an electrical field. In this second sense, it also occurs in the definition of the "diffusion length" of the carriers, i.e., the mean distance the carriers travel by diffusion.

5. Efficiency
   The percentage of input solar radiation which is converted by the solar cell to useful electrical energy.

$$\text{Efficiency}(\%) = \frac{\text{cell output} \times 100}{\text{solar input for total area (including contacts)}}$$

6. Evaporation Masks
   Contacts and coatings for solar cells are generally applied by thermal evaporation in vacuo. The areas where these contacts or coatings are required are defined by shadow masks, with appropriate openings, held in close contact with the solar cell surface during evaporation.

7. I-V Characteristics
   The numbers used to define the current-voltage output from a solar cell. The output is measured as a continuous curve (traced by varying the load resistance from zero to infinity) in the fourth quadrant of the complete I-V curve. The most often used terms are:

   Short Circuit Current (I_{SC})
   The current generated by the incident light when the cell terminals are shorted.

Open Circuit Voltage (V_{oc})
The voltage developed by the light at the open terminals of the cell.

Maximum Power (P_{max})
The maximum product of load current times load voltage. The corresponding values of load current and voltage are designated I_{max} and V_{max}. Often for convenience in large scale tests, cells are graded according to the current at a test voltage close to V_{max}, e.g., for 10 ohm-cm resistivity, current is measured at 430 mV (I_{430})

Curve Fill Factor (CFF)
P_{max} expressed as a fraction of the power given by the product $I_{sc} \cdot V_{oc}$

$$CFF = \frac{P_{max}}{I_{sc} \quad V_{oc}}$$

8. Intensity
The term specifying the amount of solar energy incident on the cell. The units generally used are mW/cm^2.

9. Junction (PN)
The dividing region between the shallow surface layer and the starting silicon. The PN junction is a rectifier (diode) and is necessary for the conversion process of sunlight into electrical energy.

10. Junction Depth
The thickness of the shallow surface layer on a solar cell. This depth is generally low, typically 0.5 um.

11. N or P Silicon
Silicon can be doped with impurities to give either N (negative) or P (positive) type of conductivity. The addition of subscripts e.g., N+ or P+ is used to show that regions are heavily doped with the impurities.

12. Photovoltaic
The developing of a voltage (electrical) by a photon (light) input.

13. Radiation
A term covering the particles (electrons, protons or neutrons) or electromagnetic radiation (ultraviolet, X-Rays) which the solar cells encounter in space missions.

14. Radiation Resistance
A qualitative term describing how well solar cells can withstand the exposure to radiation. The term can be made quantitative by defining the percentage of output power remaining after a given dosage by a specified radiation.

15. Saturation Current
The theoretical current associated with the diode created by the PN junction. Ideally, it is the current collected by the junction from carriers generated by thermal processes at the cell operating temperature.

16. Schottky Barrier
A potential barrier arising at the interface between a metal and a semiconductor, such as silicon. It is named after the German scientist who first explained these barriers.

17.. Sheet Resistance
The resistance of a unit square of a thin layer of material such as the surface layer of silicon in solar cells. It depends both on the sheet thickness (junction depth) and the carrier concentration in the surface layer.

18. Solar Simulator
A test setup which illuminates solar cells by the solar spectrum for specific missions. The defining parameters are the spectrum (AMO for space sunlight) and the intensity (e.g., 140 mW/cm^2 for near-earth, 5 mW/cm^2 for near-Jupiter.)

1.0 SUMMARY

1.1 Program Objectives

The contract objective was to develop silicon solar cells for use on spacecraft missions covering a heliocentric orbit range of 0.1 to 15 astronomical units.

The purpose of the program was to exploit the present state-of-the-art variables available for N/P silicon solar cells. These variables are the base resistivity of the P-silicon, the PN junction depth, the sheet resistance, the grid contact configuration, the contact metals and the coating. The variables were to be combined in fabricating cells designed for five specific missions, namely for orbits near Mercury, Venus, Mars, the Asteroid belts and Jupiter.

Probable operating conditions were chosen for each of the five orbits. From these conditions, cell designs were determined, using a combination of contemporary solar cell theory and previous measurements on cells designed to operate within this range of orbits.

Using these mission designs, a fabrication sequence was chosen for the cells, and groups of cells were fabricated. These mission design cells were intended for measurement at conditions simulating the various missions, and their performance compared to that of two groups of "control cells" made according to the best present near-Earth optimized cells.

In addition to the mission design cells, an alternate approach was included, aimed at finding cells with good performance at some of the five target missions. This alternate approach used a sixteen-position matrix of cell designs, combining fairly wide ranges of four cell fabrication variables, namely bulk resistivity, PN junction depth, back contact metals and the number of grid contacts.

1.2 Theoretical Analysis

The first part of the program was theoretical analysis. Using the solar intensity expected near the various orbits and making plausible assumptions, the equilibrium temperatures were calculated.

Analysis was made of the solar cell properties at the various combinations of intensity and temperature. This analysis was based on three sources, namely, present solar cell theory, published theoretical analyses of various missions and practical cell measurements covering some of the range of interest. These latter measurements were needed to provide guidelines for cell

parameter variations which were not predictable from the theoretical analysis. The results of the analysis are incorporated in Table 1 which specifies the various cell parameters chosen for the cells designed for the five missions. The parameters used for optimum near-Earth orbits are also included.

1.2.1 Design of Cells for the Inner Missions (Mercury, Venus)

The design problems resolved to reducing the total series resistance of the cell to very low levels to reduce parasitic losses from the large generated currents. Key cell parameters were chosen to ensure low series resistance. Thus low resistivity silicon ($\sim$1.0 ohm-cm) was used, a deeper PN junction ($\sim$ 0.7μm) with corresponding lower sheet resistance ($\sim$20 ohm/square) and grid configurations providing good current pickup. In addition, in order to keep the cell operating temperature low, a large sacrifice in possible output was needed. The temperature reduction resulted from use of front surface (grid) contacts which reflected a large portion of the input power. For example, for Mercury cells, 60% of the incident power was reflected, leaving less than half the normal active cell area.

A theoretical analysis showed no overall advantage in shifting the maximum of the reflectivity curve by increasing the thickness of the antireflection coating.

1.2.2 Design of Cells for the Outer Missions (Mars, Asteroid belts, Jupiter)

For these missions, the lower solar intensity leads to lower cell temperatures than for Earth orbits and the inner orbits. In addition, the power loss due to series resistance is significantly reduced because of the lower current generated. The two main causes for cell power loss are:

(a) Possibility of a Schottky voltage barrier at the back surface interface between the P-silicon and the contact metals. This barrier is most likely to form at lower temperatures, i.e., it is more serious as the spacecraft sun distance increases.

(b) Excess leakage currents in the PN junction. These currents can arise for several reasons during processing. These reasons include surface preparation damage, diffusion-induced strains, introduction of harmful impurities, or damage from mechanical handling.

The practical solution to (a) was to include a P+ layer on the P-silicon, to minimize the chance of forming a Schottky barrier. This P+ layer was provided by both

TABLE 1

CELL PARAMETERS FOR MISSION-DESIGN CELLS

Mission	Resistivity (ohm-cm)	Junction Depth (μm)	Sheet Resistance (ohm/sq)	Front Contact	Back Contact	Grid * Configuration	Anti-Reflective Coating	Comments
Mercury	0.8-1.5	0.6	20	Ti-Ag	Ti-Ag	Checkerboard or 4 wide grids	SiO	Must have low series resistance Can connec to any edg
Venus	0.8-1.5	0.5	25	Ti-Ag	Ti-Ag	10 grids	SiO	Must have low series resistance
Earth	0.8-1.5 7-14	0.4 0.4	33 45	Ti-Ag Ti-Ag	Ti-Ag Ti-Ag	6 grids 6 grids	SiO SiO	
Mars	1-3	0.6	20	Ti-Ag	P+ with Ti-Ag	4 grids	SiO	
Asteroid Belts	3-7	1.0	15	Ti-Ag	P+ with Ti-Ag	2 grids	SiO	Need extra care in preparatio of front surface an edges, and in contact sintering.
Jupiter	3-7	1.0	15	Ti-Ag	P+ with Ti-Ag	1 grid	SiO	Need extra care in preparatio of front surface an edges, and in contact sintering.

Grid Patterns shown in Figures 15, 16

P+ diffusion or by alloying of aluminum. The latter method was more convenient, and was adopted.

There was no such ready solution to (b). Extreme care was needed in silicon surface preparation, in diffusion techniques, and in the handling steps. Also, care was taken to reduce the sintering temperature time cycle to prevent the chance of punch-through of the PN junction by the contact metals. In addition, higher resistivity silicon (3-7 ohm-cm) was used because the PN junction quality could be higher. Deeper junctions were used to afford additional protection from surface leakage.

The grid contact analysis, although not so important, was extended to these outer missions and the optimum number of grids for Mars, the Asteroid belts, and Jupiter were derived as four, two and one, respectively.

1.2.3 Solder Coverage

It was considered best for all missions to reduce the amount of solder used, or preferably to eliminate it altogether on the cells. This is practical because several interconnecting methods are available which do not require solder on the cells.

1.3 Mission-Design Cell Fabrication

Based on the parameters in Table 1, the starting silicon, diffusion, contact and coating parameters were controlled and combined to give cells designed for the five missions. Cell groups are described in Section 5.1 below. A total of 1300 cells was made for these groups.

1.4 Matrix Cell Fabrication

Sixteen groups of cells were made using extreme values of resistivity (0.1 and 10 ohm-cm), junction depth (0.4 and 1.6μm) combined with two grid configurations (zero or six) and two back contact structures. The matrix scheme is given below in Section 5.2.

As described below, the first matrix cells were accidentally mixed during fabrication. A second run was made for all sixteen groups. For both runs, a total of 3200 cells was made, with 100 control cells.

1.5 Cell Measurements

The cells described above were measured at 28°C under the following illumination conditions:

(a) 140 mW/cm^2, AMO spectrum

(b) 5 mW/cm^2, AMO spectrum (used a perforated box as neutral filter)

(c) 850 mW/cm^2, Tungsten Iodide illumination

Cell Measurements (continued)

(d) Dark (zero illumination) forward diode characteristics

(e) Dark (zero illumination) reverse diode characteristics

(f) Typical spectral response at 28°C

The results of these measurements are given in Section 6.2 below.

In addition, typical cells from each group were to be measured at:

(i) 850 mW/cm^2, cell approximately 100°C

(ii) 5 mW/cm^2, cell at -140°C

(iii) Dark forward diode characteristics, -140°C

As explained below, these latter measurements were not performed. They will be completed after this report, and the results will be reported separately.

1.6 Fabrication of Deliverable Cells

Based on the measurements, the final design for cells optimized for five missions was decided, and the deliverable cells (5 groups, 50 cells) were fabricated. These cell groups are described in section 5.3 below. Two additional groups were added and are described. For these seven groups at least 1400 cells were fabricated.

1.7 Conclusions

The program, including theoretical analysis, cell fabrication, and analysis for 28°C measurements, led to conclusions which were incorporated in the cells designed for the target missions, and are described above.

Final conclusions will be made separately from this report, based on simulated mission measurements to be made in the future.

Some general conclusions are possible, as follows:

(1) Present-day cell processing techniques can be varied and combined to give cells theoretically capable of good operation for the target missions. The outer missions presented more difficulty in cell design.

(2) There is often unexpected interaction between cell fabrication steps when these are varied over fairly wide range. Such interactions must be understood and minimized before the separate effects of these variations can be found. Present methods used to analyze cell properties are adequate to explore these interactions.

(3) The precise blend of cell parameters cannot be finalized without taking into account all the mission requirements.

1.8 Significant Program Development

The current literature and previous measurements were incorporated into the theoretical analysis. This analysis showed that present range of available cell parameters should give cells designed for the five target missions. The cell fabrication steps showed reasonable trends in cell properties measured at 28°C. It also appeared that currently available analytical methods (combining photovoltaic I-V characteristics, dark I-V characteristics, spectral response and physical measurements) are adequate to check the effects of the variations in cell processing steps. The program provided relatively large samples (up to 100 per group) in about thirty cell groups covering a wide range of parameters. These cells will add to existing cell measurement information.

The development not completed when this report was written was the final simulated mission evaluation and analysis. This phase will be completed in the future and the results will be reported separately.

2.0 INTRODUCTION

2.1 Document Organization

This report consists of the following major parts:

(a) A summary (Section 1.0) of the program objectives, the work accomplished, and the conslusions drawn.

(b) Background material (Section 2.0) to explain the Program chosen.

(c) The detailed work plan (Section 3.0).

(d) A theoretical analysis (Section 4.0) of cell performance over the range of expected conditions.

(e) Fabrication details of optimized cells (Section 5.0).

(f) Details of measurements made (Section 6.0), and analysis of these measurements.

(g) Conclusions drawn (Section 7.0).

(h) Suggestions for future work (Section 8.0).

(i) References (Section 9.0).

(j) A bibliography of pertinent references, with notes. (Section 10.0)

(k) Appendix A, describing the special test equipment.

2.2 Purpose and Objectives

The purpose of the program was to exploit the present state-of-the-art for N/P silicon solar cells to design and fabricate cells optimized for each of five separate missions covering the range of orbits near Mercury (to 0.1 astronomical units) out to near Jupiter (to 15 astronomical units).

Five specific missions, namely near the orbits of Mercury, Venus, Mars, the asteroid belts and Jupiter, were chosen as specific targets.

The objectives of the program were to survey previous work, to combine these results with present understanding of silicon solar cell operation, and to design specific cells optimized for the five missions. Following fabrication of the cells, detailed measurements and analysis were performed, and conclusions drawn as to the effectiveness of the program.

2.3 Background to Program

Most silicon solar cells fabricated have been optimized for near-earth orbits. Thus they perform well at intensities around 140 mW/cm^2, and cell temperatures from 10 to 60°C. Some modification in cell design (often drastic) is required when designing for orbits with intensities as low as 5 mW/cm^2 and temperatures around -140°C, or for intensities up to 850 mW/cm^2, and cell temperatures around 100°C. Cells designed specifically for these extremes (Jupiter and Mercury missions) have been built and analyzed. However, it was thought profitable to examine the whole range of missions over which the importance of various controllable cell parameters could change and to combine these parameters to give cells optimized for the five missions under study.

At the outset, it was agreed that all of the necessary array systems requirements e.g. low weight, and low cost could not be included in this study. However, the cells designed are comparable to present systems suggested for these missions and in a few cases (e.g. light weight, large area arrays for Jupiter) any advancements in array design could probably include the cell improvements suggested in the present program.

No allowance was made for radiation resistance. In the case of the inner missions, nearer the sun, the only radiation of concern is sporadic solar flares, and these can be partly dealt with by combination of transparent shielding (covers) and by the chance of accelerated annealing at higher cell operating temperatures. For the outer missions, the main problem is from the Jovian radiation belts, and no ready solution exists for the suspected intense irradiation at low cell temperatures, while maintaining the low weight of a large area array.

Previous related work on cell parameter measurements within the present range of interest is summarized by listing the references, with notes on the highlights of the conclusions drawn. In some cases the work referenced is proceeding simultaneously with the present program.

3.0 PROGRAM PLAN

3.1 Program Tasks

The tasks accomplished in the program arose from work outlined in the preceding sections. These tasks are summarized in the following sections.

3.11 Analysis Phase

Most of the pertinent literature references were read and information considered useful for the present program was extracted. A list of these references with notes is given in Section 10.0 below. In addition to these published results, in-house measurements at Centralab Semiconductor were analyzed over the range of interest. These measurements showed how conventional cells begin to lose their effectiveness as the extremes of high or low solar intensity were approached. Based on the conclusions from these previous measurements, current solar cell theory was used to derive designs which should give optimum performance at the various target missions.

3.12 Cell Fabrication Phase

The fabrication sequence was similar to that used for conventional cell manufacture except that the initial silicon resistivity, P/N junction diffusion, contact materials and the masks used were varied according to the scheme shown in Table 1. The process flow chart is shown in the next section.

3.12.1 Process Flow Chart

The fabrication sequence used for the cells made was as follows:

1. Grow silicon single crystal of required resistivity, and P-type obtained by adding boron dopant.

2. Cut the crystal ingot into 2x2 cm slices, using O.D. diamond saws for major shaping, and I.D. diamond saws for slicing.

3. Lap and polish one side of the slices, using in-house machines. The final polish is by a combination mechanical-chemical method ensuring very good optical finish with low work damage.

4. Clean the slices for diffusion

5. Diffuse wafers, producing a shallow, highly-doped N- silicon layer. The wafers are heated in a tube furnace, and inert carrier gases with addition of phosphorous oxychloride carry the dopant over the slices.

6. By etching remove the diffused layer from the non-polished side of the slice, to expose P-silicon.

7. Clean the slices for contact evaporation. This involves removing the phospho-silicate glass layer remaining on the polished surface after diffusion.

8. Place slices in a vacuum evaporator with the P-side facing coils from which Titanium (Ti) and Silver (Ag) are thermally evaporated. The system pressure is reduced below a control point, and the amounts of metal deposited are controlled by resistance monitoring. When required an additional coil containing aluminum (Al) is used.

9. The slices are placed in fixtures in the evaporator with the polished N+ side in contact with a mask which has openings to produce the required grid contact structure. Metals are evaporated as in 8 above.

10. The slices are placed in another evaporator, and held to expose the active area. Silicon monoxide is then evaporated into this surface. The amount of SiO is controlled by a quartz crystal monitor.

11. The slices are sintered in a reducing atmosphere (hydrogen) at near 600°C for around 5 minutes.

12. The slices are compressed between inert spacers with the edges exposed. The excess metals and the damaged silicon layers around these edges are removed by chemical etching.

13. At this stage if required, cells can be solder coated, either wholly or by use of masking materials, only in preselected areas.

14. Also if required, the solder coating can be reduced in thickness to below 1 mil by an additional solder-pressing operation, in a machinespecially designed for this purpose.

15. The cells are inspected for mechanical defects.

16. The cells are now ready for electrical testing.

The different grid pattern masks used in step 9 above were designed in Centralab and purchased from an outside supplier.

In addition to cells optimized for specific missions, the sixteen groups of cells comprising the matrix test were fabricated. The scheme for these matrix cells is given in Section 5, Table 6.

3.13 Measurement Phase

As cells were made, measurements were taken on the solar simulators at 140 mW/cm^2. Also, for cells at 28°C, two special light sources were set up, one using a perforated box to give 5 mW/cm^2 when placed under the simulator, the other a source consisting of a tungsten iodide lamp capable of providing 850 mW/cm^2. At 28°C, dark forward and dark reverse diode I-V characteristics were recovered. Also typical spectral response curves were drawn, using a set of ten narrow band filters between a tungsten light source and the cells.

Work was begun on simulating actual conditions for the Mercury and Jupiter missions, but these measurements were not completed.

During, or after, cell fabrication, measurements were made of physical parameters such as bulk resistivity, sheet resistance and P/N junction depth.

3.14 Analysis of Measurements

Measurements on the various groups allowed extraction of the average values and the spread in P max., Isc and Voc. The dependence of these I-V characteristics on the fabrication parameters, was studied. The results are given below in Section 6.2.

3.2 Program Changes

The program had several changes from its original plan. There was a delay in finishing the analysis phase, because of the need to combine empirical results with the theoretical analysis.

A change from the original contract was the addition of the sixteen matrix groups, their fabrication and measurement. As mentioned above, the first 1600 cells fabricated for the matrix cells were mixed during processing, requiring an additional 1600 cells to be made. A good deal of time was wasted in testing these mixed matrix cells.

The testing phase was curtailed because of personnel reduction in the Centralab Solar Measurements Group. Thus the originally intended testing program was not completed.

After discussion with JPL, it was agreed that specific mission conditions could be simulated on the JPL equipment, and typical cells from the optimized cell groups as well as some matrix cells would be submitted to JPL. Thus the analysis and cell fabrication portions were completed, but the originally planned measurements at actual mission conditions were not made during the contract period.

There were also changes in the delivery and scope of reports, mostly resulting in the incorporation of all essential details in this Final Report.

4.0 ANALYTICAL STUDY OF OPTIMIZED DESIGN FOR SOLAR CELLS

The analysis was divided into two parts, namely for near-sun missions, inside earth-orbit, and far-sun missions, outside earth-orbit. The inner missions are discussed in Section 4.1, the outer missions in Section 4.2.

4.1 Near-Sun Missions

4.1.1 Temperature Calculations

The equilibrium temperature of a solar cell in space depends upon its own thermal characteristics and upon the incident power. Rather than begin with a set of assumed temperatures for the five conditions under study, the temperatures were calculated using the equation:

$$T^4 = \frac{\alpha}{\epsilon_1 + \epsilon_2} * \frac{S \cos \phi \ (1-n)}{D^2 \sigma} \qquad (1)$$

where

α = front surface solar absorptance (0.81)

ϵ_1 = front surface hemispherical emittance (0.84)

ϵ_2 = assumed back surface emittance (0.9)

S = solar constant at D=1 (0.136 W-cm^2)

D = solar distance in astronomical units (Earth=1)

σ = Stefan-Boltzmann constant (5.6686 x 10^{-12} watts-cm^{-2}-deg^{-4}

ϕ = angle of incidence (0, cos ϕ = 1)

T = temperature (°K)

n = solar cell efficiency

The front surface solar absorptance of typical covered solar cells is 0.81 and the front surface total hemispherical emittance at 300K is 0.84. The emittance has a slight temperature coefficient (2×10^{-4}/K) but this will be ignored.

The cells are assumed to be mounted on a paddle type structure. For this configuration we may assume an effective back surface total hemispherical emittance

of 0.9. This is consistent with temperature differentials actually experienced on honeycomb substrates and with published emittances of black high emittance finishes. The solar constant is taken as 0.136W-cm^2, a realistic value in light of recent measurements (Reference 1). If a solar constant value of 0.1396W-cm^2 is preferred, the equilibrium temperatures for Mercury and Venus increase by 2-3°C.

The angle of incidence is assumed to be 0 (normal incidence). The power generated by the solar cells mounted on a paddle type structure is generally dissipated elsewhere in the spacecraft. This has the effect of lowering the solar temperature.

The efficiency is based upon total cell area, and values ranging from 0.01 at Mercury to 0.16 at Jupiter (as shown in Table 2), were estimated from the measured values for Earth and Jupiter. The choice of the efficiency value need not be more precise because T is governed by $1/4\sqrt{1-n}$. For example, assuming the extreme n-values of 0.16 or 0.01 for a given mission will only cause 4% difference in the calculated temperature. In addition, D will vary according to the mission, trajectory, and the α and ϵ values can only be specified to within a few percent.

TABLE 2

Calculated Equilibrium Temperature

Orbit	Solar Distance (Au)	Solar Flux ($mW-cm^{-2}$)	Assumed Efficiency	Temperature (°C)
Mercury	.39	894	0.01	246.1
Venus	.72	262	0.06	104
Earth	1.0	136	0.10	43.5
Mars	1.52	59	0.12	-17.6
Asteroid Belts	2.77	17.7	0.14	-85.1
Jupiter	5.2	5	0.16	-136.9

4.1.2 Temperature Reduction for Mercury Missions

The calculated temperature for a conventional cell at Venus (104°C) is reasonable, and worthwhile amounts of power can be expected. However, this conventional cell will be essentially inoperative at Mercury because of the high equilibrium temperature. It is necessary to reduce the input energy by some means to bring the temperatures to a reasonable level.

Several methods have been proposed to limit the input energy to a solar cell for operation at Mercury (Reference 2). Tilting the solar panel is one approach, where cos ϕ in Equation 1 is reduced. This method has an advantage in that full power can be available during the entire mission, but the spacecraft attitude control to maintain proper orientation at Mercury is difficult. Another method is to limit the incident energy by reflecting a portion of it (reducing α_s in Equation 1).

This reflection can be done in either of two methods:

(1) Use of a bandpass filter to accept radiation where the cell is most efficient, and

(2) Use of a spatial filter, where a portion of the area of the cell reflects the sunlight.

The bandpass filter approach is better theoretically, but practical filters fall somewhat short of ideal filters used in calculations. The spatial filter technique is easily applied and has a secondary benefit in that the reflecting portion can also be used as a contact material and thus reduces series resistance in the cell. This approach has been selected for development.

4.1.3 Cell Power Studies

The optimization of the reflecting contact cell is best carried out with a digital computer. The successful application of a computer requires an equation relating cell power to cell temperature and irradiance, and an equation relating cell temperature to irradiance and thermal characteristics. The latter equation is Equation (1) in Section 4.1.1. The former has been derived using earlier data.

As a starting point, the series of curves shown in Figure 1 was used. These curves were derived from a series of measurements on Centralab 1 x 2 cm cells and can be applied to 2 x 2 cm cells directly. The curves were drawn at a constant temperature (28°C) by bonding the cell to a water-cooled heat sink and monitoring temperature with a thermocouple. The source was a

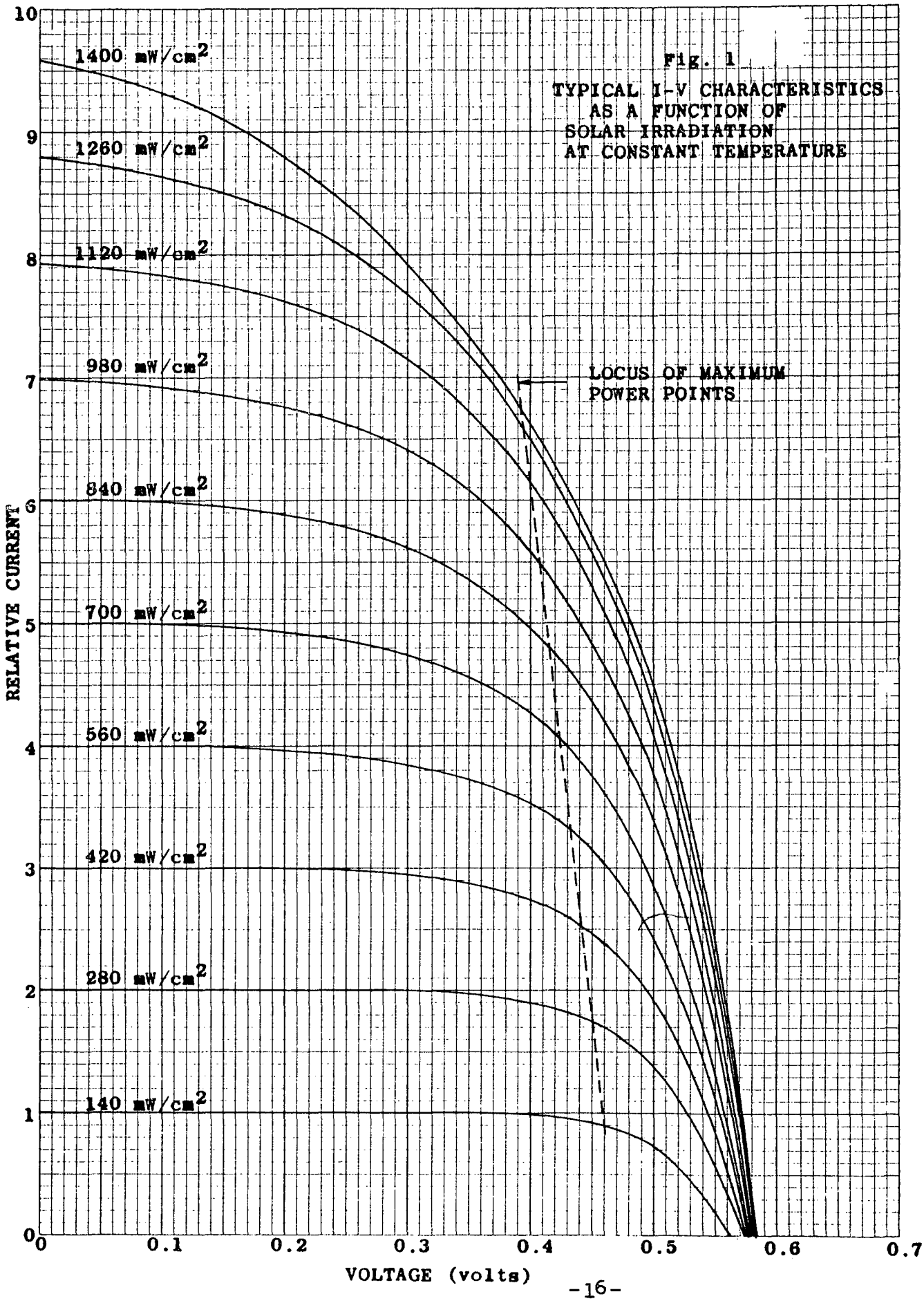

Fig. 1
TYPICAL I-V CHARACTERISTICS AS A FUNCTION OF SOLAR IRRADIATION AT CONSTANT TEMPERATURE

filtered 1000 watt tungsten landing lamp and the radiation was focussed on the cell with a large parabolic reflector. The I-V curves were made using a variable voltage source such that they could be drawn well into the reverse region. This enabled the cell under test to be its own irradiance detector, by scaling the light-generated current I_L to multiples of the I_L at AM=0, 1AU. The series resistance effect of the test leads was mathematically removed from the original curves.

To determine the effect of temperature on these curves, the voltage axis was shifted in 100mV increments to a total shift of 400mV. Using a temperature coefficient of open circuit voltage of -2.26mV/°C, these shifts correspond to temperatures of 72, 117, 161 and 205°C. in addition to the original curves at 28°C. The small change in current was neglected in order to simplify the calculations.

The maximum power for each of the five temperatures and for irradiances of 1 to 8 AM=0 suns was determined from the curves using transparent overlays and slide rule calculations. The powers determined (relative) are shown in the following table.

TABLE 3

Relative Power at Various Irradiances and Temperatures

Suns / Temp (°C)	1	2	3	4	5	6	7	8
28	.414	.787	1.116	1.434	1.726	1.992	2.232	2.456
72	.324	.612	.862	1.105	1.320	1.528	1.702	1.871
117	.236	.439	.617	.790	.937	1.090	1.206	1.321
161	.149	.278	.389	.493	.584	.690	.765	.834
205	.073	.138	.193	.243	.286	.343	.381	.412

The values in the table were plotted as the ordinate with the irradiance as the abcissa and the temperature as the parameter. The plots are not linear, so a "range of interest" was devised such that the expected temperature and irradiance levels would be included. Within this "range of interest", straight line approximations can be made. The graph is shown in Figure 2. Five equations were derived, one for each temperature. They are

$$28°C \quad - P = .331S + .123$$
$$72°C \quad - P = .245S + .123$$
$$117°C \quad - P = .169S + .099$$
$$161°C \quad - P = .101S + .086$$
$$205°C \quad - P = .04S + .092$$

where P is the relative power and S is the irradiance in solar constants.

A graph was made, plotting the coefficient of S and the ordinate intercept against the temperature T as shown in Figure 3. A second-order polynomial was fit to the coefficients of S using the values at T=28, 117 and 250°C. This polynomial is ($2 \times 10^{-6}T^2 - 2.11 \times 10^{-3}T + .389$). For the ordinate intercept a least squares straight line was fitted, taking the form ($-2.23 \times 10^{-4}T + .13$). The factor 143 was added to convert the relative value at 28°C, AM=0 (0.414) to 59mW. The complete equation is

$$P=143\left[S(2\times10^{-6}T^2-2.11\times10^{-3}T+.389)+.13-2.24\times10^{-4}T\right] \qquad (2)$$

P = power in mW from a 2 x 2cm cell

S = solar constants

T = cell temperature (°C)

The equation fits the measured data rather well. The solid triangles in Figure 2 show solutions to the equation for various values of T and S.

A program incorporating the two equations was written in the BASIC language for the General Electric MKII time-sharing computer. A fraction (X) of the cell area was assumed covered by a reflecting grid with a solar absorptance of 0.1. The solar absorptance of the cell active area was assumed to be 0.85. Previous trials indicated that the optimum value of X lay between 0.55 and 0.70, so X was varied between these limits in 0.01 increments. It was assumed that the final power was

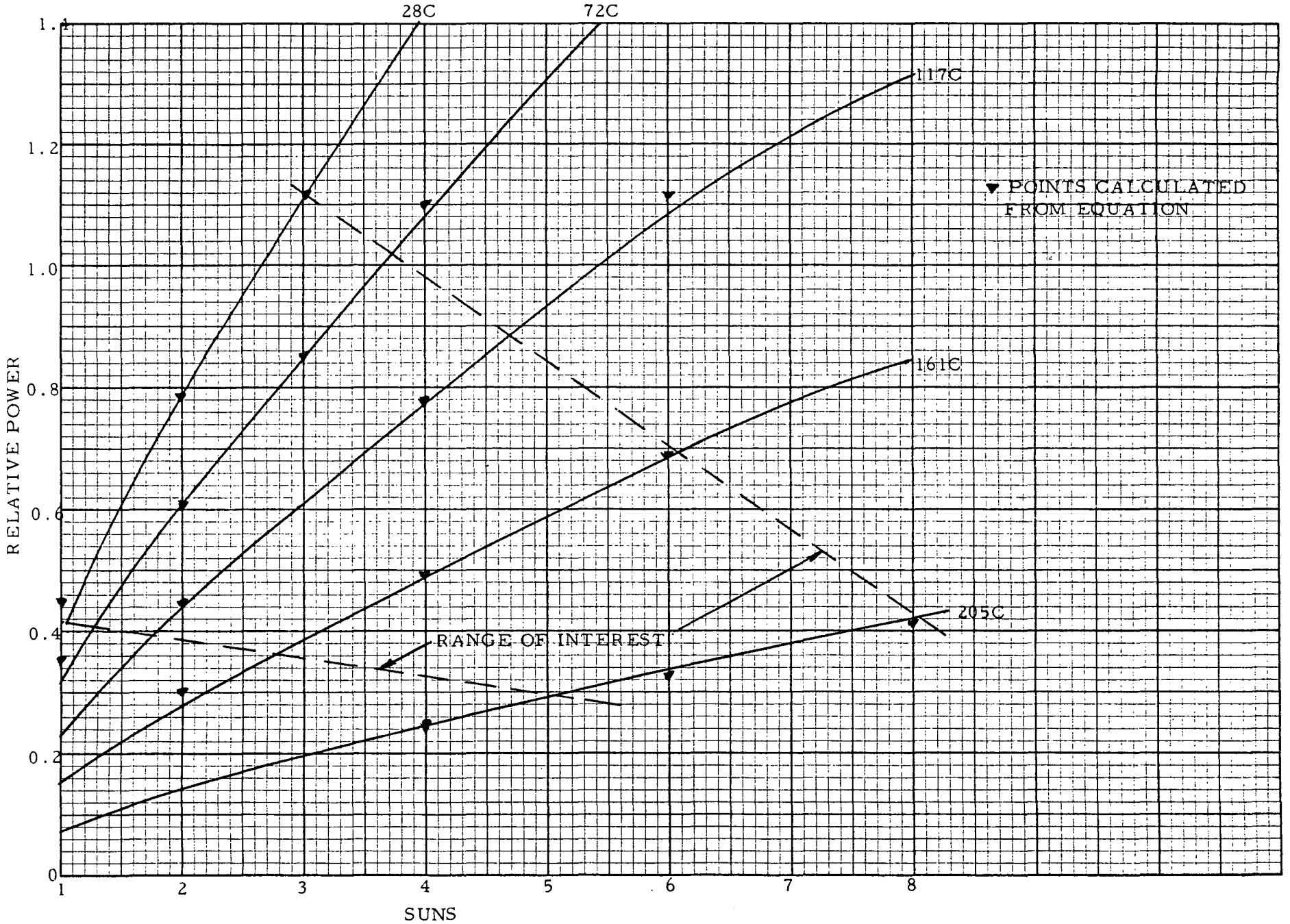

FIGURE 2. RELATIVE POWER vs. IRRADIANCE and TEMPERATURE

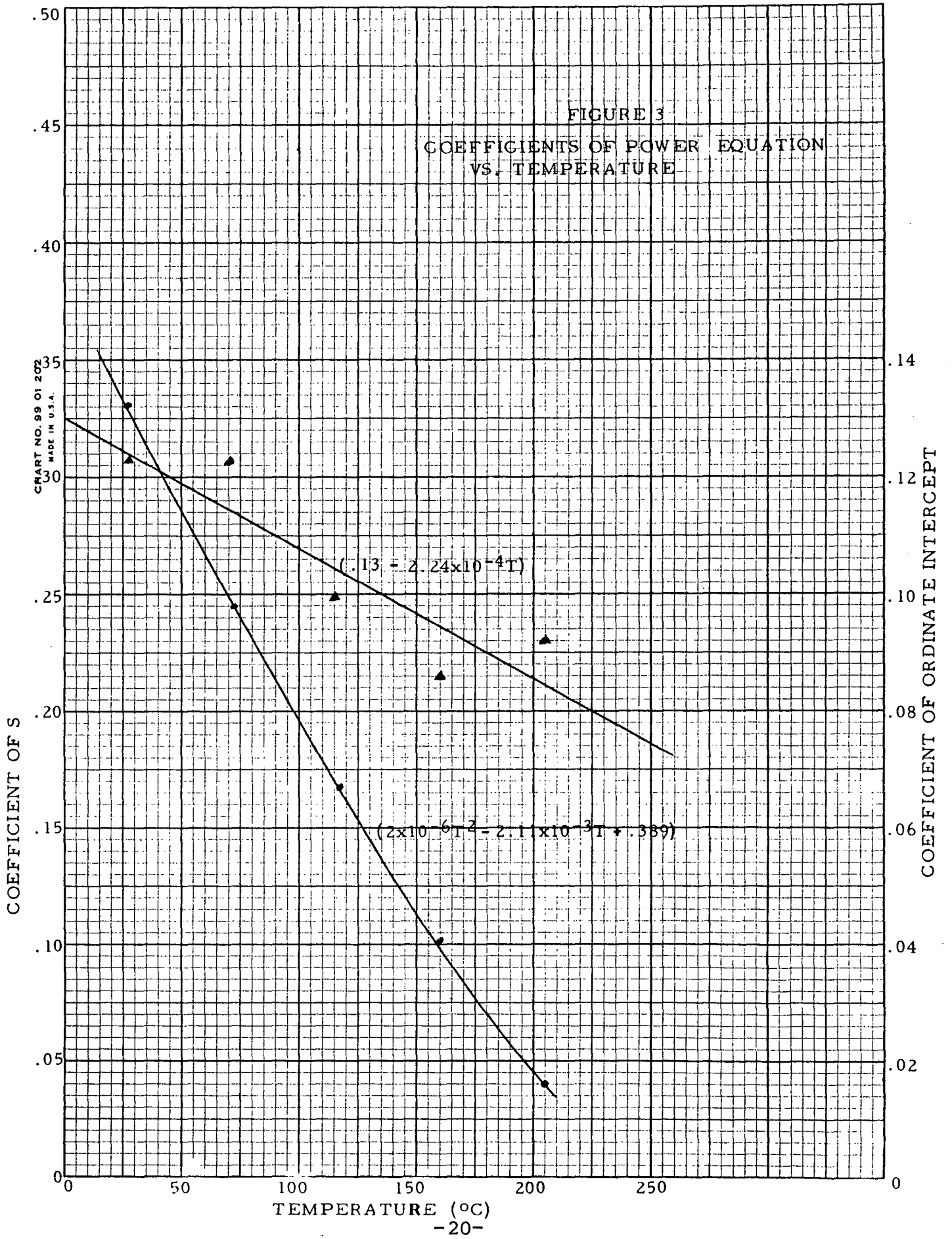
FIGURE 3
COEFFICIENTS OF POWER EQUATION
VS. TEMPERATURE
(.13 - 2.24x10⁻⁴T)
(2x10⁻⁶T² - 2.11x10⁻³T + .389)
COEFFICIENT OF S
COEFFICIENT OF ORDINATE INTERCEPT
TEMPERATURE (°C)
.50
.45
.40
.35
.30
.25
.20
.15
.10
.05
0
.14
.12
.10
.08
.06
.04
.02
0
0
50
100
150
200
250
CHART NO. 99 01 202
MADE IN U.S.A.

directly proportional to the fraction of the exposed area. The results of these calculations are shown in Table 4.

TABLE 4

Output Power vs Fraction of Cell Covered

Fraction Covered (X)	Temp. (°C)	Power (mW)
.55	168.2	44.26
.56	166.3	44.44
.57	164.3	44.59
.58	162.4	44.70
.59	160.4	44.78
.60	158.4	44.82
.61	156.3	44.83
.62	154.3	44.81
.63	152.2	44.75
.64	150.0	44.65
.65	147.9	44.51
.66	145.7	44.33
.67	143.5	44.11
.68	141.2	43.84
.69	138.9	43.54
.70	136.5	43.19

By inspection of the table, it can be seen that the optimum reflective area is 0.61, with a resulting equilibrium temperature of 156.3° and a power of 44.83mW. It can also be seen that for the power to be within 1% of optimum, the reflective area fraction can vary between .56 and .66. When the same analysis was applied for D = .72 (Venus), it showed an optimum reflecting area of 0, indicating temperature control by this means is not needed at Venus.

4.14 Series Resistance

For operation at high levels of irradiance such as a Mercury or Venus mission, the most important loss factor is the series resistance. Consequently, for these missions the series resistance must be minimized. Assuming that contact resistances are not improveable beyond the currently used titanium-silver system, the two elements of importance are the diffused layer-grid structure resistance and the bulk resistance. Since some 61% of the top surface of a Mercury cell must be reflective, a contact pattern can be derived using the reflecting area to minimize the series resistance.

As a starting point, Equation (3) (Reference 2) was modified:

$$S^3 + \left(\frac{2W^2}{T} * \frac{P_T}{P_s} + \frac{3T}{2}\right) S^2 + \left(4W^2 * \frac{P_T}{P_s}\right) S - \frac{4VT}{P_s j_{mp}} = 0 \quad (3)$$

where S = grid separation

W = cell width (1.9cm)

T = grid line thickness

P_t = sheet resistance of grid line

P_s = sheet resistance of diffused layer

V = cell voltage at operating temperature (190mV)

j_{mp} = cell current density at operating point (.26 A/cm^2)

The relationship $T = 1.22S/(.78-S)$, which was derived from the area constraint was used. The resulting equation, a third order polynomial, was solved for a combination of diffused-surface sheet resistances and grid-line sheet resistances using a ROOTER program in the GE time-sharing library. The results, shown in the table below, indicate a 3 or 4 grid cell would be optimum if Equation (3) applies.

TABLE 5

Optimum Grid Numbers for Mercury Cells for Various Cell Parameters

P_t Ω/□	P_s Ω/□	S (cm)	T (cm)	N
.005	40	.17	.38	3.3
.005	30	.20	.47	2.7
.005	25	.22	.54	2.3
.005	20	.25	.65	1.9
.002	40	.17	.39	3.2
.002	30	.20	.48	2.6
.002	25	.22	.55	2.3
.002	20	.25	.66	1.9

Values of .005 and .002 ohms per square grid line resistance correspond to unsoldered and soldered titanium-silver grids. The N values are the number of grids calculated from the relationship $N=(2-S)/(S+T)$. This number must be rounded up to the next higher integer and S and T re-evaluated. Figure 4 shows a four-grid Mercury cell according to this criterion.

It is evident from inspection of Figure 4 that a more desirable grid pattern could be devised, leaving the same reflecting area and putting on more grids. Equation 3 is useful for optimizing a grid pattern where the active area is unknown, but it apparently does not apply in this case. In an attempt to arrive at a useful cell for Mercury, other configurations were investigated. The most promising solution lies in a "checkerboard" pattern, as depicted in Figure 5. The active areas are quite small, and the cell is symmetrical, with orientation during assembly and testing unimportant.

For a Venus cell, Equation 3 was successfully applied to arrive at a cell with 10 grids. In this case, a gridline width of .02cm was chosen, along with a voltage of 0.3 volts and a J_{sc} of .075 A/cm^2. The calculations are shown in the table below.

TABLE 6

Optimum Grid Number for Venus Cells

P_t Ω/□	P_s Ω/□	S cm	N
.01	30	.154	10.6
.005	30	.178	9.2
.002	30	.198	8.3
.01	20	.165	9.9
.005	20	.196	8.4
.002	20	.223	7.3

The cell design is shown in Figure 6.

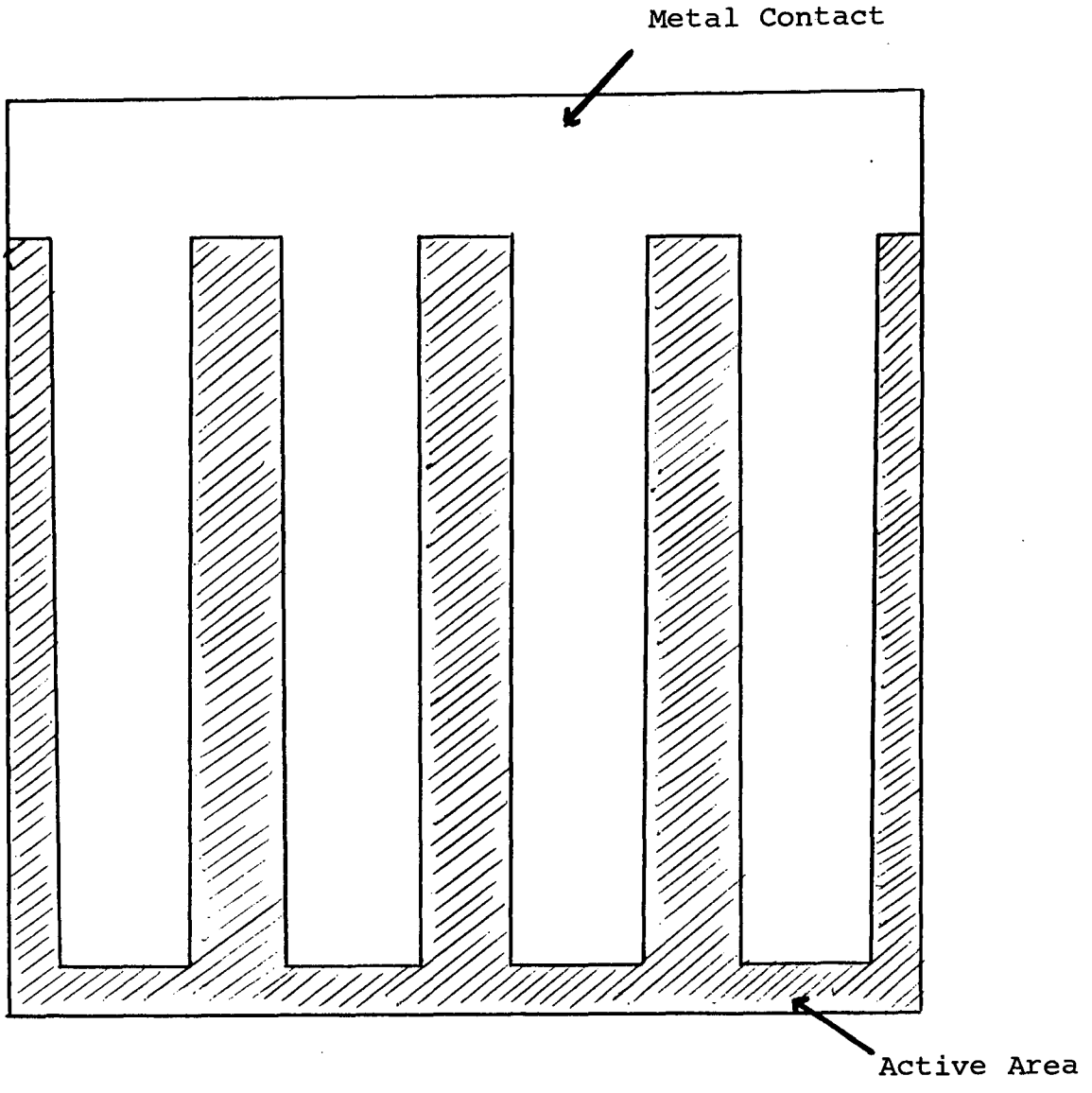

FIGURE 4

FOUR-GRID MERCURY CELL

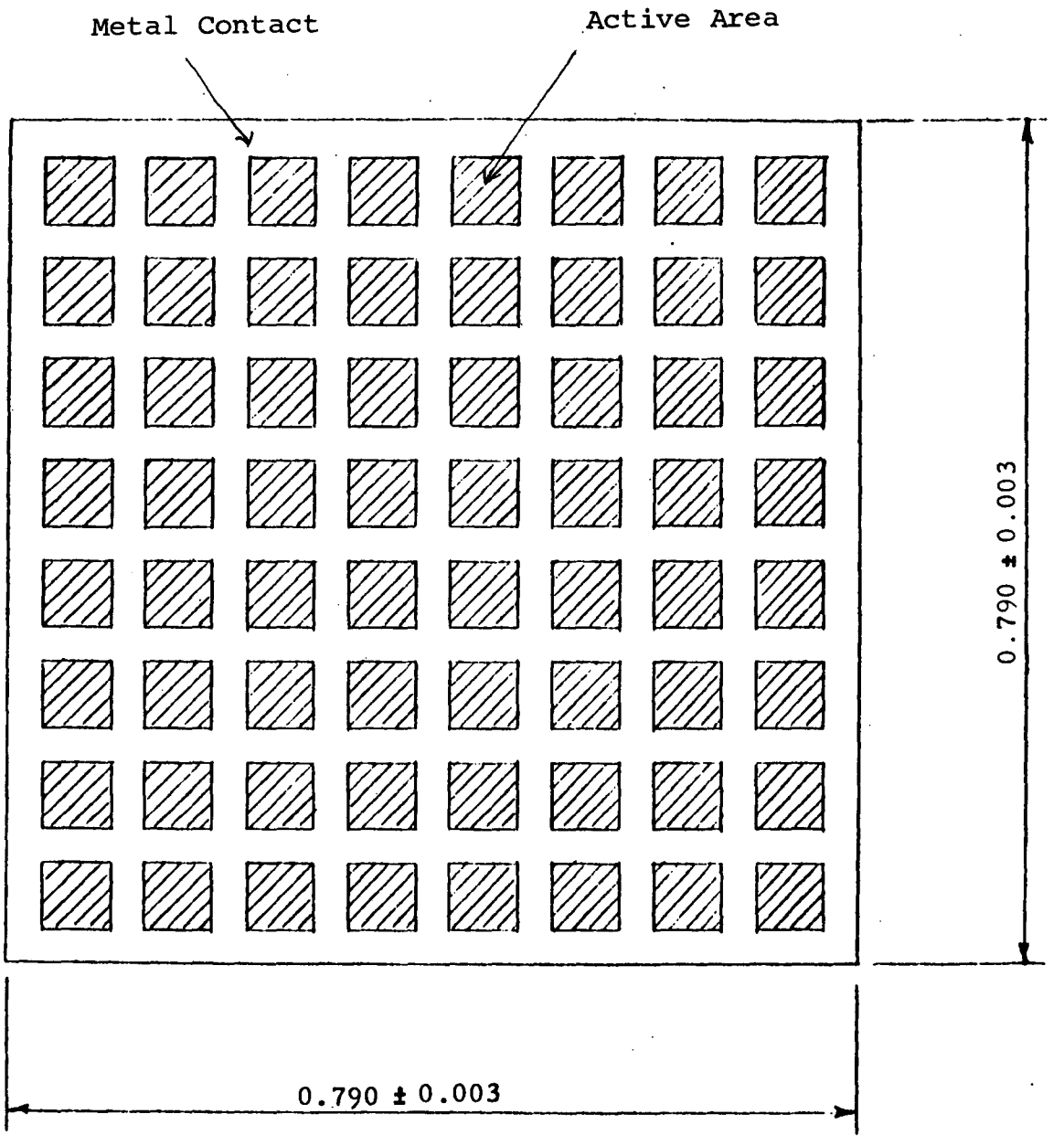

EACH ACTIVE AREA 0.060 x 0.060
SPACING 0.035

FIGURE 5

CHECKERBOARD CONTACT MERCURY CELL

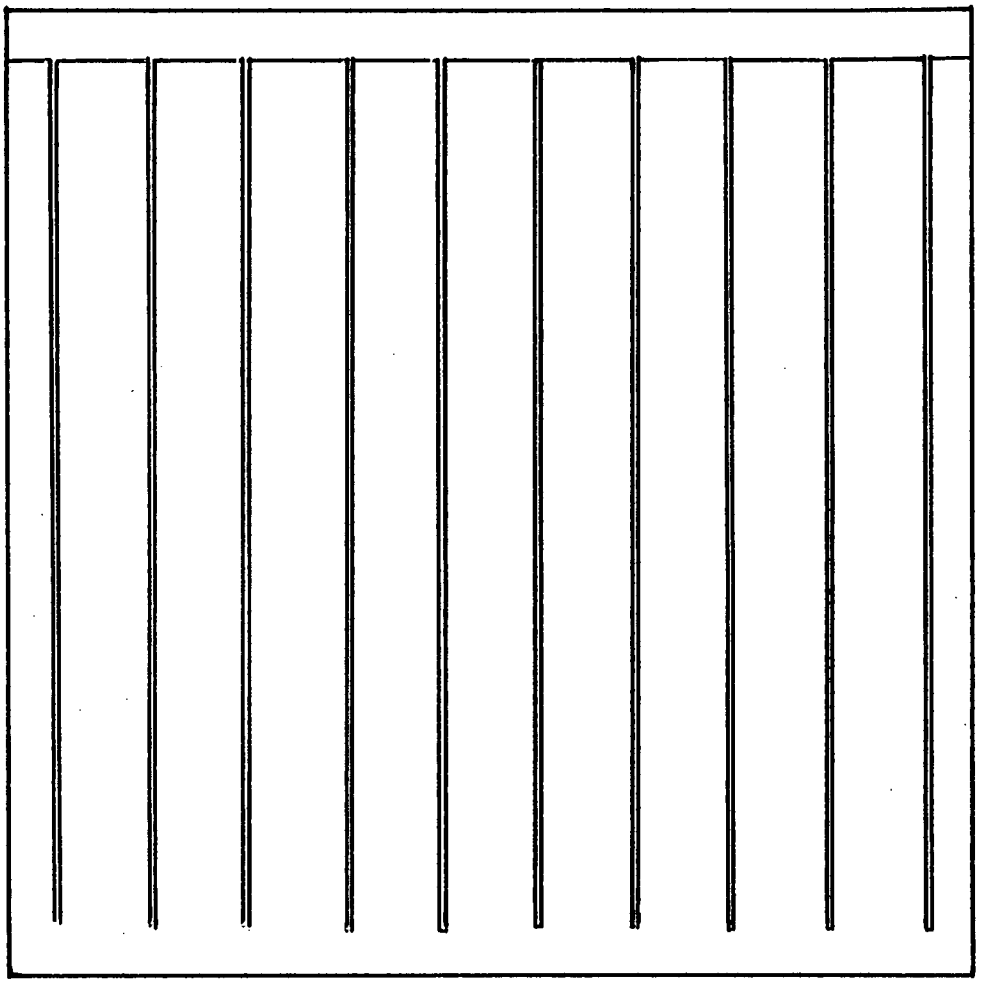

FIGURE 6

GRID PATTERN FOR VENUS CELL

The optical and electrical characteristics of the diffused layer are not sufficiently understood to allow a mathematical optimization. As the sheet resistance is decreased from 33 ohms per square (the empirically determined value for 1AU), the series resistance and the light-generated current both decrease. The change in series resistance is calculable and has been included in the grid optimization studies. The loss in current is not calculable and must be determined by experiment. Starting values of 20 ohms per square for Mercury and 25 ohms per square for Venus were selected based on earlier measurements of the loss of current. These values represented good tradeoff between I_{sc} loss and series resistance decrease.

The base resistivity is in part responsible for the series resistance of a cell, contributing about .05 ohms for a 2 x 2 cell with 10 ohm-cm base resistivity and about .01 ohms for a similar cell with 2 ohm-cm base resistivity. At a current level of 300mA (for a Venus cell) each .01 ohm of base resistance creates a voltage drop of 3mV equivalent to 1% in power. At a current of 400mA (for a Mercury cell with 61% reflective), each .01 ohm of base resistance creates a voltage drop of 4mV, equivalent to 2.1% in power. Hence, a low base resistivity is desirable. Theory indicates that lowering the base resistivity to 0.1 ohm-cm or even lower should produce good cells, with the important advantage of high open-circuit voltage. In practice, the expected voltage increase has not materialized. A few experimental cells near 0.5 ohm-cm have proven good, but these have been the exception, and even at these resistivities the expected increase in V_{oc} was not observed. Based upon present state-of-the-art, base resistivities in the range 0.8 - 1.5 ohm-cm are suitable for both Mercury and Venus cells, because the bulk silicon contribution to the series resistance can be reduced adequately without severely decreasing I_{sc}.

4.1.5 Effect of Shifting Reflection Minimum to Longer Wavelengths

It was mentioned earlier that a bandpass filter offered theoretical advantages for reducing the input energy to a Mercury cell. An hypothesis was formulated wherein the reflection minimum of the SiO anti-reflection coating normally applied to solar cells would be shifted to longer wavelengths where the efficiency of solar cells is higher and would lower the temperature by reflecting some of the less useful short-wavelength solar radiation with a net increase in power. The currently used SiO thickness is 8×10^{-8}m (800 Å) corresponding to a reflection minimum of approximately 6×10^{-7}m (6000 Å).

Calculations were made to determine solar absorptance and power loss due to decreased film transmission for film thickness from 7×10^{-8}m to 12×10^{-8}m (700Å to 1200Å).

The variation in solar absorptance with film thickness was calculated using equations giving reflectance as a function of component indices of refraction and thickness, applied at 20 selected ordinates (Ref. 4). The reflectance equations (Ref. 5) are

$$R = \frac{r_1^2 + r_2^2 + 2r_1 r_2 \cos 2\phi}{1 + r_1^2 r_2^2 + 2r_1 r_2 \cos 2\phi} \qquad (4)$$

where $r_1 = (n_o - n_1)/(n_o + n_1)$

$r_2 = (n_1 - n_2)/(n_1 + n_2)$

R = reflectance of assembly

n_o = index of refraction of air

n_1 = index of refraction of SiO

n_2 = index of refraction of Si

$\varphi = 2\pi n_1 e/\lambda$

e = thickness of SiO

λ = wavelength

Assuming that the assembly does not transmit any radiation, the absorptance is given by A=1-R. The computer was used to solve Equation 4 for the 20 selected ordinates using index of refraction values shown in Figure 7 (Refs. 6-8) and for film thicknesses from 700Å to 1200Å. As shown in Table 7, the temperature (calculated using Equation 1) does indeed drop with increasing film thickness, and the relative power due to this temperature drop (calculated using Equation 2) does increase.

TABLE 7

Temperature and Relative Power for Various SiO Thicknesses

Sio Thickness (nm)	λ For R min (nm)	Solar Absorptance (s)	Equilibrium Temperature (°C)	Relative Power	Power Loss Due to Coating	Overall Power
70	532	.839	151.2	.988	.992	.980
80	608	.834	150.2	1	1	1
90	684	.826	149.8	1.005	.989	.994
100	760	.822	149.4	1.009	.966	.975
110	836	.820	149.1	1.013	.937	.949
120	912	.813	148.4	1.021	.908	.927

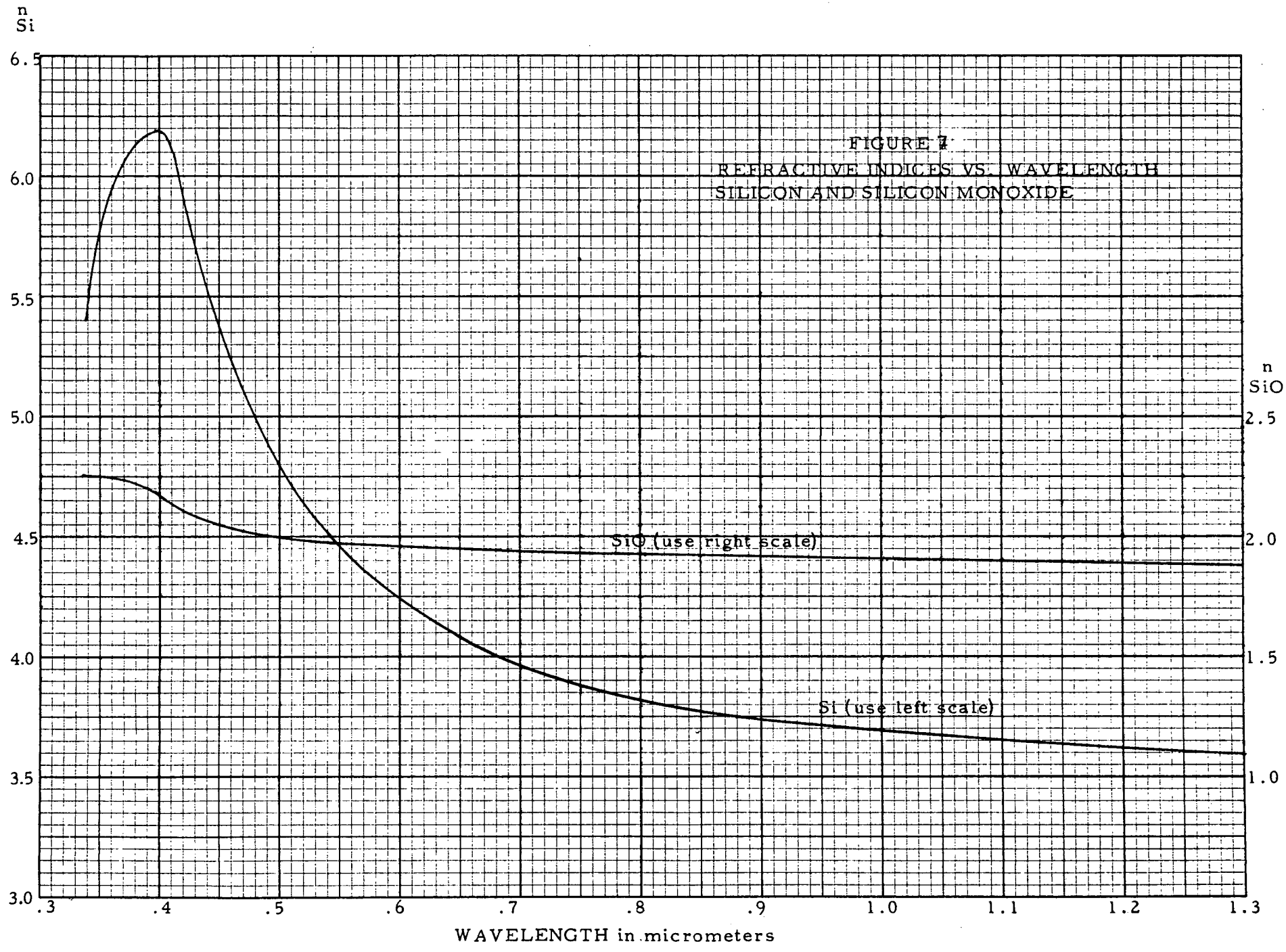

FIGURE 7
REFRACTIVE INDICES VS. WAVELENGTH
SILICON AND SILICON MONOXIDE

However, there is a loss in light-generated current due to the increased reflection of light in the wavelength range where the sunlight is most intense. This is demonstrated by the reflectance curves shown in Figure 8. To determine the magnitude of this loss, a short computer program was written wherein the spectral response of a bare (uncoated) cell was multiplied by both Johnson's curve and the ratio of (1-R) of the coated cell to (1-R) of bare silicon. The results were summed across the spectral range of the cell. Mathematically, this is given by

$$I = \Sigma_{J_{(\lambda)}} * R_{(\lambda)} * \frac{1-R_{1\ (\lambda)}}{1-R_{2\ (\lambda)}} \qquad (5)$$

where I = current

$J_{(\lambda)}$ = solar spectral irradiance (Johnson)

$R_{(\lambda)}$ = relative response of uncoated cell

$R_{1(\lambda)}$ = reflectance of uncoated cell

$R_{2(\lambda)}$ = reflectance of coated cell

These results are also shown in Table 7, wherein the relative power is equated to I in Equation 5. When the two relative powers are multiplied, it is apparent that no net gain is achieved by altering the anti-reflective coating.

4.1.6 Cell Designs

This section describes the cells designed for Mercury and Venus applications. All aspects of their design have been considered. A summary of the parameters used was given in Table 1.

Base Resistivity and Type:

a. Mercury - 0.8 to 1.5 ohm-cm, boron doped

b. Venus - 0.8 to 1.5 ohm-cm, boron doped

Junction Characteristics:

a. Mercury - 20 ohms/sq ($\sim 6 \times 10^{-5}$m) phosphorus

b. Venus - 25 ohms/sq ($\sim 5 \times 10^{-5}$m) phosphorus

FIGURE 6

ANTI-REFLECTION COATING CHARACTERISTICS

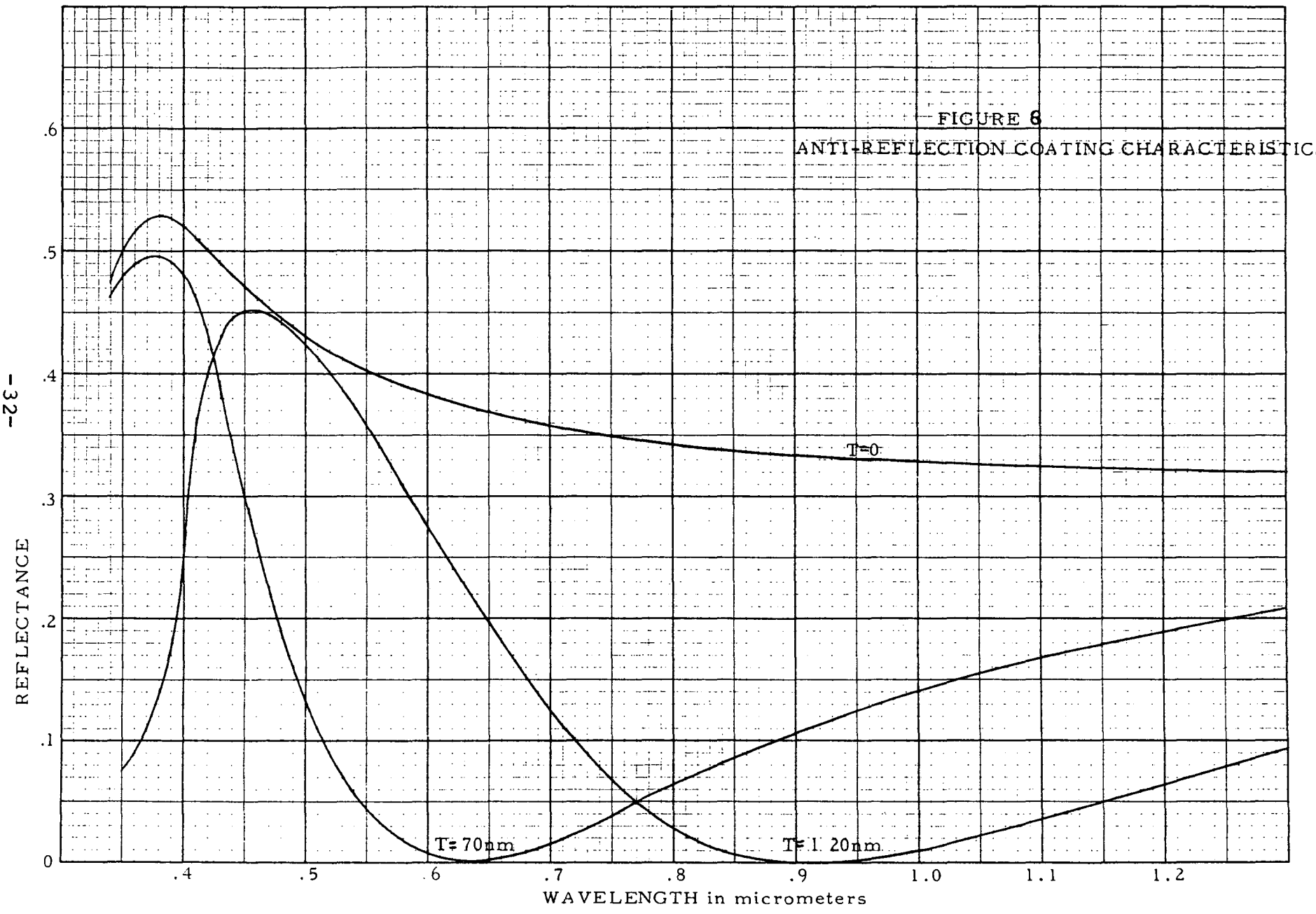

Contact Material:

a. Mercury - sintered titanium-silver, solderless

b. Venus - sintered titanium-silver, solder optional

Grid Pattern and Size:

a. Mercury - see Figure 5

b. Venus - see Figure 6

Anti-reflective Coatings:

a. Mercury - 8×10^{-8}m (800Å) SiO

b. Venus - 8×10^{-8}m (800Å) SiO

Handling Characteristics and Restraints:

a. Mercury - no restraints. Since cell is symmetrical, it can be used with any edge as the contact.

b. Venus - no restraints. Handle like conventional cells.

Production Cost and Implementation Time:

a. Mercury - the cost of the Mercury cell will be slightly greater than conventional cells because one additonal evaporation is required. The implementation time will be the same as for other cells, being limited only by acquisition time of evaporation fixtures.

b. Venus - the cost of the Venus cell will be similar to conventional cells. The implementation time will be the same as for other cells, being limited only by acquisition time of evaporation fixtures.

Weight:

a. Mercury - same as conventional cell (2x2cmx.036cm thick), 0.35 gram.

b. Venus - same as conventional cell (2x2cmx.036cm thick), 0.35 gram; with optional solder, 0.41 gram.

Special Tooling:

a. Mercury - special evaporation mask required, 8 fingers, each 1.5mm (0.060 in.) wide.

b. Venus - special evaporation mask, similar to conventional but for 10 grids.

4.2 Outer Missions

The target missions for orbits outside earth orbit are Mars, the Asteroid belts and Jupiter. Table 2 above shows the progressively lower values of solar flux and temperature expected on these three missions.

4.2.1 Optimum Grid Numbers

The predominant cell losses change from series resistance losses which were dominant for the Mercury and Venus missions. However, there are still slight gains to be made by varying the grid line coverage, and for this, the analysis given in Section 4.14 is applied again, using equation (3) to compute the actual number of grid lines to be used for the outer missions. The computer solutions for the optimum grid patterns for the three missions are given in Tables 8 through 10. The symbols used were defined in equation (3), in Section 3.4 above.

TABLE 8

Optimum Grid Numbers for Mars Cells

for Various Cell Parameters

P_T	P_S	S	T	N
Ohms/□	Ohms/□	cm	cm	
.005	30	.418	.02	3.61
.005	35	.398	.02	3.83
.005	40	.382	.02	4.07
.002	30	.430	.02	3.53
.002	35	.409	.02	3.76
.002	40	.391	.02	3.96

TABLE 9

Optimum Grid Numbers for Asteroid Belt Cells for Various Cell Parameters

P_T	P_S	S	T	N
Ohms/□	Ohms/□	cm	cm	
.005	25	.715	.02	1.75
.005	30	.675	.02	1.91
.005	35	.642	.02	2.05
.005	40	.616	.02	2.18
.002	25	.729	.02	1.70
.002	30	.687	.02	1.86
.002	35	.653	.02	2.00
.002	40	.625	.02	2.05

TABLE 10

Optimum Grid Numbers for Jupiter Cells for Various Cell Parameters

P_T	P_S	S	T	N
Ohms/□	Ohms/□	cm	cm	
.005	25	1.149	.02	.73
.005	30	1.084	.02	.83
.005	35	1.031	.02	.92
.005	40	.987	.02	1.01
.002	25	1.164	.02	.71
.002	30	1.096	.02	.81
.002	35	1.041	.02	.90
.002	40	.996	.02	.99

From these tables it can be seen that four grids are required for the Mars mission, two for the Asteroid Belts and one for Jupiter. The various values used for grid line and diffused layer sheet resistances are also listed along with the solutions of the equation for grid separation (S).

The next sections discuss the various loss mechanisms expected at the outer mission operating conditions.

4.2.2 Effects of Decreasing Intensity

As mentioned above, the decreased intensities generate correspondingly lower current densities. The short circuit current decreases linearly with intensity if the cell is maintained at near-earth temperature ($\sim$30°C). This can be seen in Table 11 which lists the average values of I_{sc} for 70 N/P cells (of near-Earth conventional design) measured at AMO, 140mW/cm^2 (near Earth) and AMO, 5.2mW/cm^2 (near Jupiter) conditions.

TABLE 11

Effects of Decreasing Intensity for Cells at 28°C

Intensity (AMO Spectrum) mW/cm^2	140	5.2
I_{sc} (4cm^2 N/P cell) average (mA)	142	5.5
V_{oc} (4cm^2 N/P cell) average (mV)	555	455
CFF = $P_{max.}/I_{sc}$, V_{oc}	.73	.705
Conversion Efficiency %	10.3	8.5

The open circuit voltage V_{oc} also decreases with decreasing intensity when the cell temperature is held at 30°C. Table 11 compares the V_{oc} values at the two intensities, also the values of curve fill factor (CFF=max. power/I_{sc} x V_{oc}). Thus, considering intensity decreases only, the conversion efficiency of the cells would decrease slightly for cells held at near-Earth temperature, and measured at the lower intensities, as seen in the table.

The decreased V_{oc} is not predictable from the I_{sc} decrease only, probably because of detailed differences in PN diode behavior at different light intensities. This means that at present actual measurements must be made for comparison.

4.2.3 Effects of Decreasing Temperature

The effects of the lower temperatures expected for these missions have a greater effect on the cell properties, and they provide the major problems which have to be overcome in order to optimize cell output.

Not all the effects of low temperature operation are harmful. Most important, the open circuit voltage (V_{oc}) increases with decreasing temperature, and the rate of increase of V_{oc} exceeds the rate of decrease of other parameters such as I_{sc} and CFF.

Therefore, with good design, the conversion efficiency of the cell for operation on the outer missions can increase significantly and steadily, reaching the 16-18% range at Jupiter distances.

4.2.3.1 Effects of Temperature on V_{oc}

As mentioned above, V_{oc} increases as the temperature decreases. The main physical reason is the same as that causing lower V_{oc} for the higher temperature missions, namely, the change in the forbidden energy gap width (Eg) with temperature. The quoted values of $\frac{dEg}{dT}$ are -2.4×10^{-4} eV/°C. (4) The Eg change can effect V_{oc} by altering the Fermi level separation, and also by changing the diode saturation current; therefore it is not possible to predict the V_{oc} changes from $\frac{dEg}{dT}$. Measured values for $\frac{d\ V_{oc}}{dT}$ are around -2mV/°C.

There is some variation in measured values of $\frac{d\ V_{oc}}{dT}$, depending on the value of illumination intensity used to measure V_{oc}, and also depending on the background resistivity of the cell. For conventional solar cells, the energy gap does not vary much over the impurity concentration range used to make good cells, (5×10^{14} to 10^{16} impurities per cm^3) but the position of the Fermi level approaches the band gap edge more closely for higher concentrations and thus allows greater values of V_{oc} to be obtained when higher concentration (lower resistivity) silicon is used as starting material.

Figure 9 shows approximate curves for V_{oc} versus temperature for two illumination intensities and two resistivity values. Temperatures corresponding to missions of interest are noted. Other curves can be found in references 10 through 15.

These changes in V_{oc} are basic and cannot be altered by design. However, they provide one criterion from which the optimum resistivity can be chosen. From Figure 9 it can be seen that for all temperatures of interest here, lower resistivity silicon has a greater V_{oc} value although the differential decreases as temperature decreases.

4.2.3.2 Formation of Schottky Barrier

It is sometimes observed that V_{oc} does not increase steadily with decreasing temperature, and this arises from the formation of a Schottky barrier at the silicon-metal interface at the back surface of the cell.

Schottky barriers are among the oldest potential barriers used in semiconductor work, and have widespread useful applications. In the past several years, great improvements have been made in controlling and measuring the properties of various metal semiconductor barriers. In the present work the Schottky barrier becomes appreciable at lower temperatures, and under illumination, can provide a photovoltage opposed to the main P/N junction, and thereby decreases the available V_{oc} of the cell. Although unusual, such Schottky barriers have even been observed at near-Earth temperatures as a result of cell processing.

For example, N/P cells with titanium-silver contacts do not normally have appreciable Schottky barriers. However, after dip soldering, Schottky barriers giving photovoltages above 30mV can form, leading to a "solder degradation" in cell properties. In this case, the mechanism of barrier formation is metallurgical and involves interaction of the solder components and the Ti-Ag with the silicon surface. The remedy found for operation around 30°C was either to alter the treatment of the silicon surface before evaporating Ti-Ag or to provide a highly doped layer at the back silicon surface. Schottky barriers are lower generally as the doping level in the semiconductor is increased, and therefore the addition of a highly doped like-impurity is an effective means of minimizing barrier formation at all temperatures.

For low temperature operation it is therefore necessary to ensure that the back silicon surface is highly doped immediately next to the lowest metal layer of the back contact system. In practice, several ways of doping (diffusion, alloying or ion implantation) are available. For example, a separate diffusion procedure can be introduced during cell fabrication to leave a thin, highly doped like-impurity on the exposed bulk of the cell. If this is done before the main P/N junction

diffusion, the back surface layer must be masked during the P/N junction diffusion. If it is done after the P/N junction diffusion, it is even more important that the P/N junction surface be masked. For both cases, care is needed to ensure that the additional diffusion step does not impair the perfection of the bulk silicon, thereby decreasing the final value of minority layer diffusion length.

Formation of the highly doped layer by alloying is possible at lower temperatures than diffusion. In this case a metal layer containing like doping impurity is deposited on, and alloyed into, the cell back surface. This alloy step can be performed before or combined with the contact metal deposition.

Thus, use of an aluminum layer on the P-silicon, with an alloy heating cycle included in the cell fabrication, is a convenient way to minimize Schottky barrier formation, and has been used here in the fabrication of cells designed for the outer missions.

The addition of a P+ layer to N/P cells allows the V_{oc} to continue increasing with lower temperatures as shown in Figure 9.

The greater V_{oc} resulting from high doping for low resistivity silicon is maintained down to Jupiter temperatures, but as mentioned above, the difference becomes less pronounced. Below it will be seen there are other reasons for preferring higher resistivity silicon, and it is convenient that the resultant penalty in V_{oc} is less than for near-Earth operation.

4.2.3.3 Effects of Temperature on I_{sc}

Three separate factors all contribute to reduced I_{sc} at lower temperature. These factors are discussed in turn in the next three sections.

4.2.3.3.1 Increasing Band Gap

I_{sc} in the solar cell arises from the intrinsic excitation by photons. In this process, all photons in the incident spectrum with energy greater than the forbidden band gap, Eg, can excite an electron from the valance band into the conduction band. As temperature decreases the band gap increases and therefore fewer incident photons can generate current. From 30°C to -140°C the variation of Eg is from 1.12 to 1.155eV, corresponding to a change in cut-off wavelength of 1.105 to 1.07μm.

By measuring the reduced area under the Johnson AMO curve which is available for intrinsic absorption as a

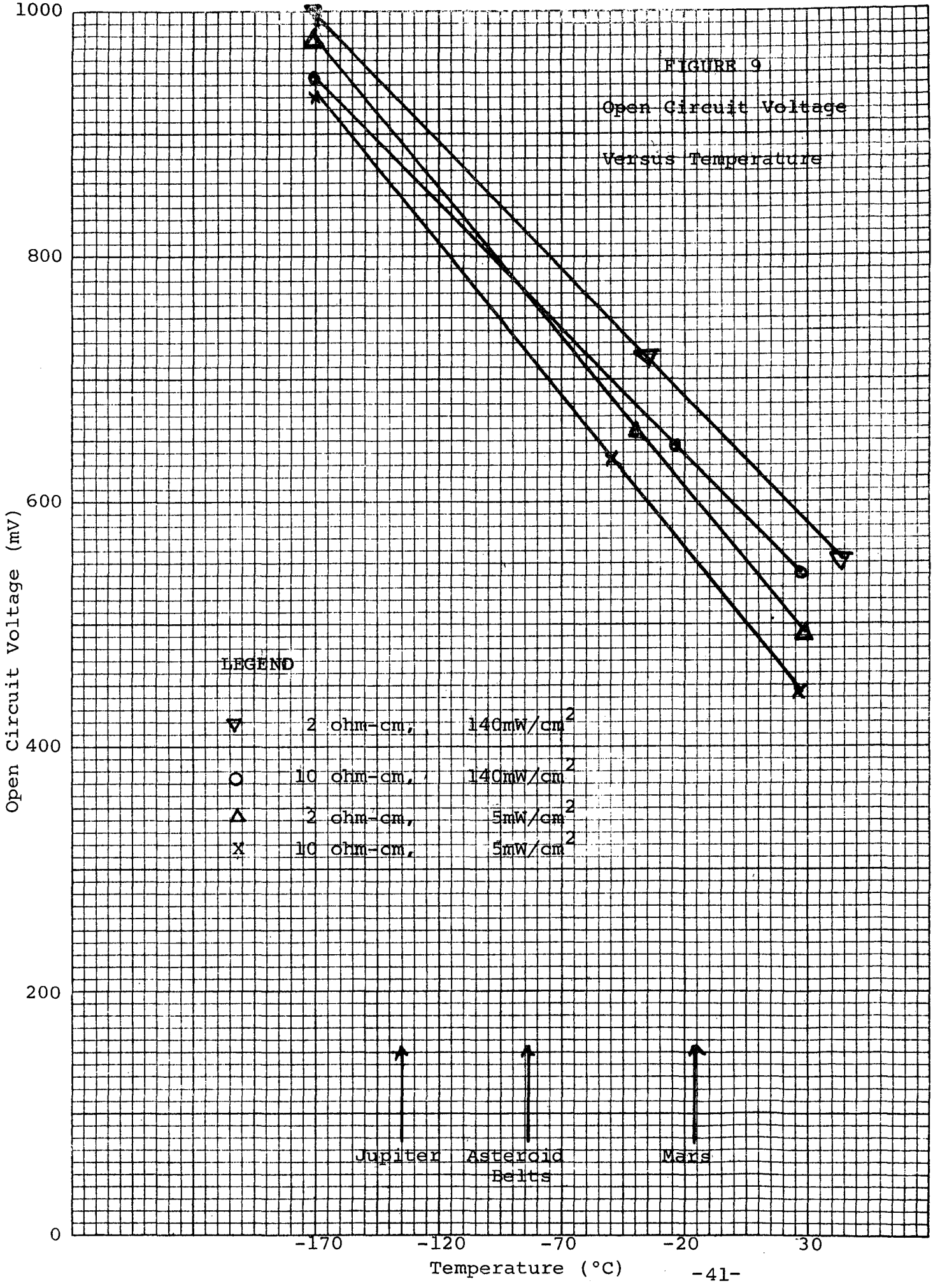
FIGURE 9
Open Circuit Voltage
Versus Temperature
LEGEND
2 ohm-cm, 140mW/cm2
10 ohm-cm, 140mW/cm2
2 ohm-cm, 5mW/cm2
10 ohm-cm, 5mW/cm2
Jupiter
Asteroid Belts
Mars
Open Circuit Voltage (mV)
1000
800
600
400
200
0
-170
-120
-70
-20
30
Temperature (°C)

result of this change of cut-off wavelength, a decrease of 2.5% in I_{sc} was estimated (see Figure 10). This loss will be the maximum expected because all the carriers generated at these longer wavelengths will not be collected at the junction.

4.2.3.3.2 Decreasing Absorption Coefficient

Current is generated as light is absorbed in the silicon. The absorption coefficient varies with wavelength, and this variation is usually combined with the variation for incident illumination with wavelength to compute I_{sc}. The absorption figures most used are those of Dash and Newman [16] and they showed that at 77°K there was less absorption than at 300°K (see Figure 11). Shumka [17] has analyzed the effects of this lower absorption on I_{sc} and calculated for temperatures from 30°C down to -40°C that $\frac{d\ Jsc}{dT}$ is about 12μA/cm²/°C. However, as mentioned below, actual I_{sc} losses are not always as high as calculated, indicating again that the collection process for carriers generated by the longer wavelengths has a large effect on I_{sc}.

4.2.3.3.3 Decreasing Diffusion Length

In addition to decreased generation of current by the effects described in the last two sections, there is also the possibility of reduced collection of the current carriers as the temperature decreases. This arises from decrease in the minority carrier diffusion length at lower temperatures. This effect has not been emphasized much in analysis of cell behavior at low temperatures but measurements show it is an important one.

Measurement of minority carrier lifetime versis temperature shows a loss of >50% as the temperature decreases from 300°K to 200°K. Extrapolation of this loss to Jupiter temperatures (130°K) shows that the loss could approach 70%. Even if the lifetime saturates at a low value it may still only be 20% of the near-Earth temperature value.

$L = \sqrt{D\tau}$ where L, D, and τ are respectively, the diffusion length, diffusion constant and lifetime for minority carriers. For the bulk region of the N/P cells, D = 39cm²/sec. and does not change drastically at lower temperatures. Thus, L decreases from 225μm to 130μm as τ decreases from 14μs to 5μs, typical of values measured at near-Earth and Jupiter temperatures respectively. Use of the curve in Figure 12, which shows AMO values of I_{sc} versus L, shows that I_{sc} could decrease from 40mA/cm² to 35mA/cm² by the time Jupiter temperatures are reached. This corresponds to I_{sc} decrease of 16%.

FIGURE 10

Effect of Decreased Temperature on Cut-Off Wavelength

A is cut-off wavelength (1.07μm) for T = 300°K

B is cut-off wavelength (1.07μm) for T = 140°K

Percent loss of absorbable spectrum (dashed portion) is 2.5%.

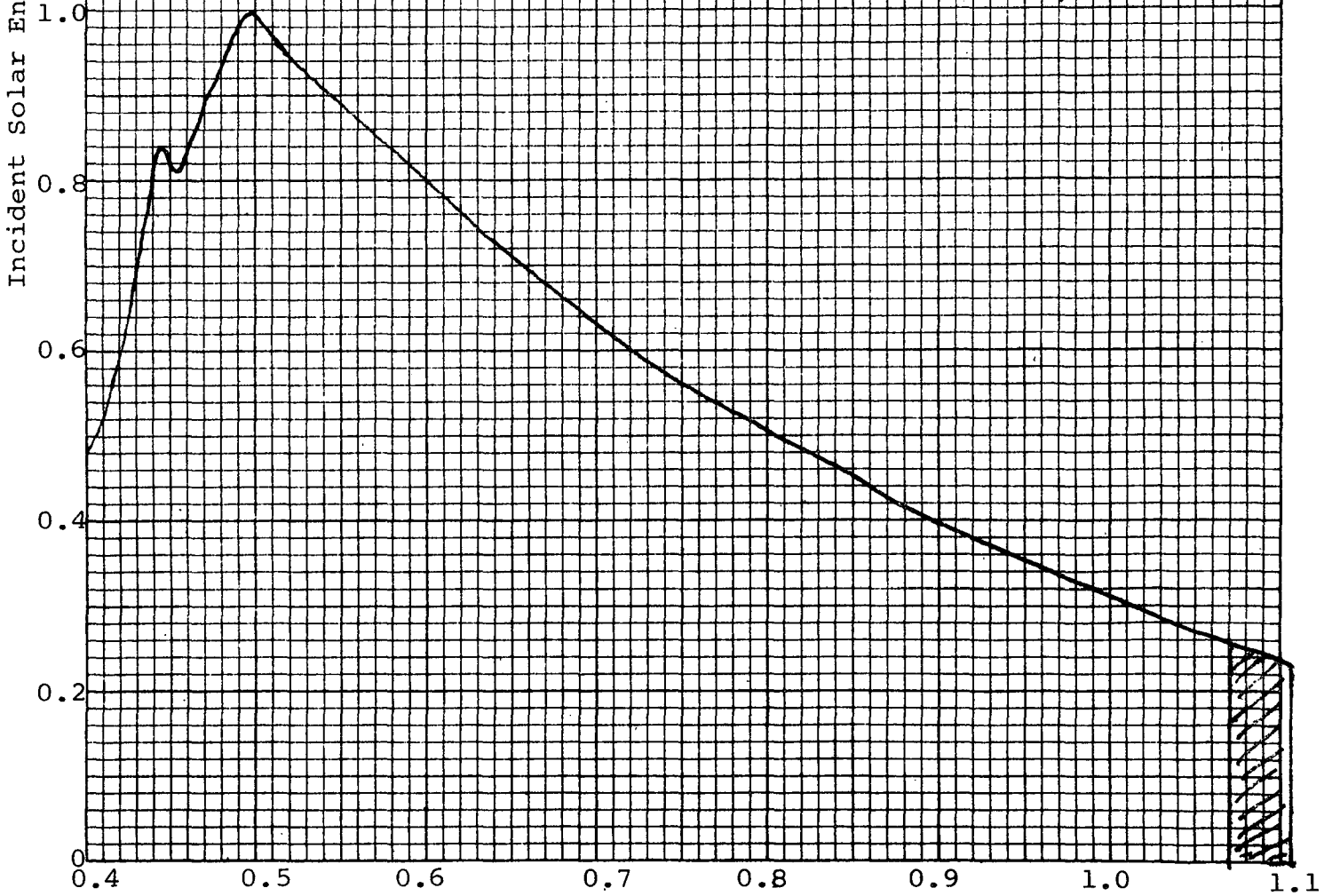

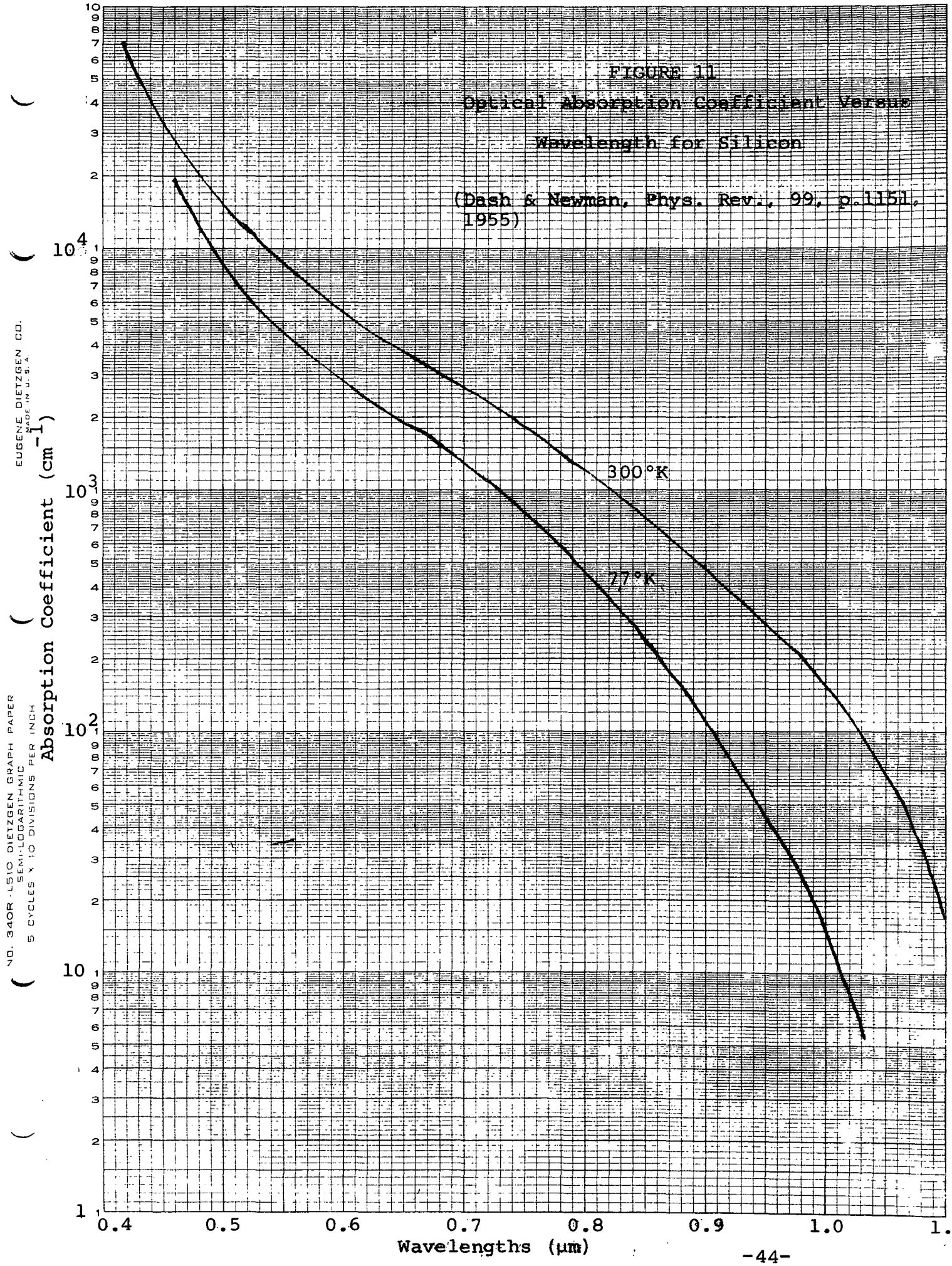
FIGURE 11
Optical Absorption Coefficient Versus Wavelength for Silicon
(Dash & Newman, Phys. Rev., 99, p.1151, 1955)
300°K
77°K
Absorption Coefficient (cm⁻¹)
Wavelengths (μm)
0.4
0.5
0.6
0.7
0.8
0.9
1.0
1.1
EUGENE DIETZGEN CO. MADE IN U.S.A.
NO. 340R-LS1C DIETZGEN GRAPH PAPER SEMI-LOGARITHMIC 5 CYCLES X 10 DIVISIONS PER INCH

[redacted] NO. [redacted] 3 C [redacted] EGEN [redacted] PH [redacted]
SEMI LOGARITHMIC
3 CYCLES X 10 DIVISIONS PER INCH

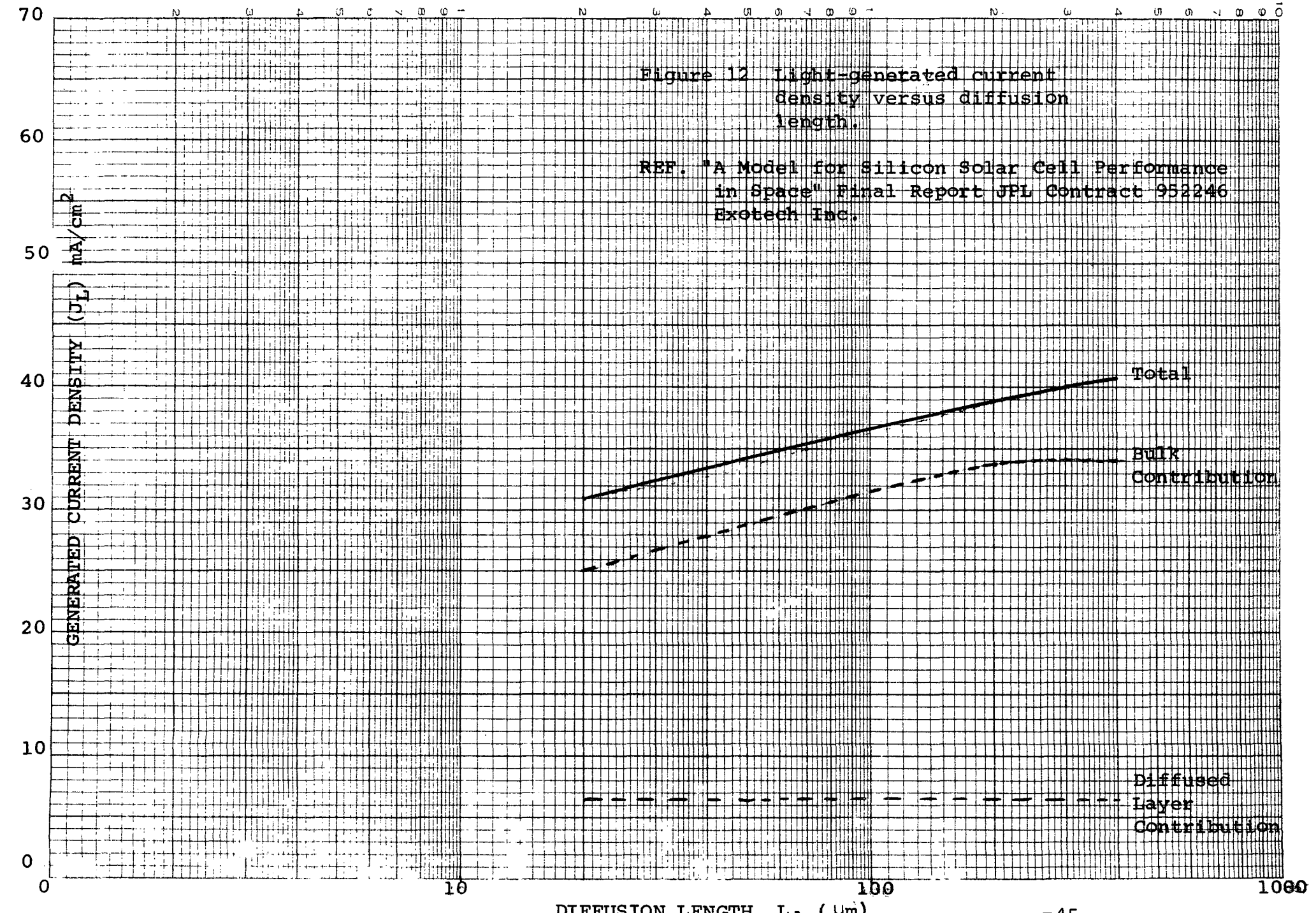

Figure 12 Light-generated current density versus diffusion length.

REF. "A Model for Silicon Solar Cell Performance in Space" Final Report JPL Contract 952246 Exotech Inc.

It is not easy to estimate the extent of the decrease of I_{sc} with temperature for a particular cell. The overall decrease can often be less than those estimated here because the measured I_{sc} losses from 20°C to -130°C for both 5mW/cm^2 and 140mW/cm^2 can be as low as 8.5%. However, the spread in I_{sc} losses was from 8.5% to 18% at Jupiter conditions, showing that the relative importance of these I_{sc} losses may vary. All three decreases in I_{sc} are most pronounced for longer wavelengths. This can be seen in the measured changes in spectral response (18). Analysis of long wavelength response of cells as a function of temperature may help to isolate the effects of the various I_{sc} loss factors.

4.2.3.4 Effects on Curve Fill Factor

One of the factors affecting CFF is the diode saturation current (I_o), CFF increasing for lower I_o (see Figure 13). As temperature decreases, I_o decreases and therefore CFF should increase. In practice, CFF is determined more by changes in the forward biased characteristics of the diode than by fundamental I_o variations. If this diode draws excess current, this reduces useful current from the cell terminals at voltages near the optimum load. Low intensity operation enhances the effects of this excess current.

The causes of excess forward current are several, and lie in the less understood properties of silicon. Often-given reasons for leaky P/N junctions include the existence of recombination centers formed in the space charge region of the diode by trace impurities or by the effects of lattice imperfections arising either from surface preparation damage or from strains introduced by the diffusion process. Other reasons include shunting of the P/N junction by leakage paths.

The extreme effects of a leaky diode are seen in low intensity, low temperature photovoltaic I-V characteristics, with the appearance of a double slope, or a pronounced flat region around the maximum power point, with an associated drastic decrease in CFF. Figure 14 compares cells with and without excess diode leakage, or Schottky barrier.

Another cause of leaky junctions arises from interaction of the shallow P/N junction and the front surface contact sintering cycle. Any surface effects are emphasized when the junction is 0.4μm deep, typical of earth optimum cells.

Interaction with the contact metals can be minimized either by changing the metals used or by reducing the sintering conditions to maintain good mechanical adhesion while reducing the chance of punch-through.

FIGURE 13

Curve Fill Factor Versus Series Resistance for Various Values of Saturation Current Density

$$C.F.F. = \frac{P_{max.}}{I_{sc} V_{oc}}$$

Assume A = 1, Shunt Resistance > 1K Ω

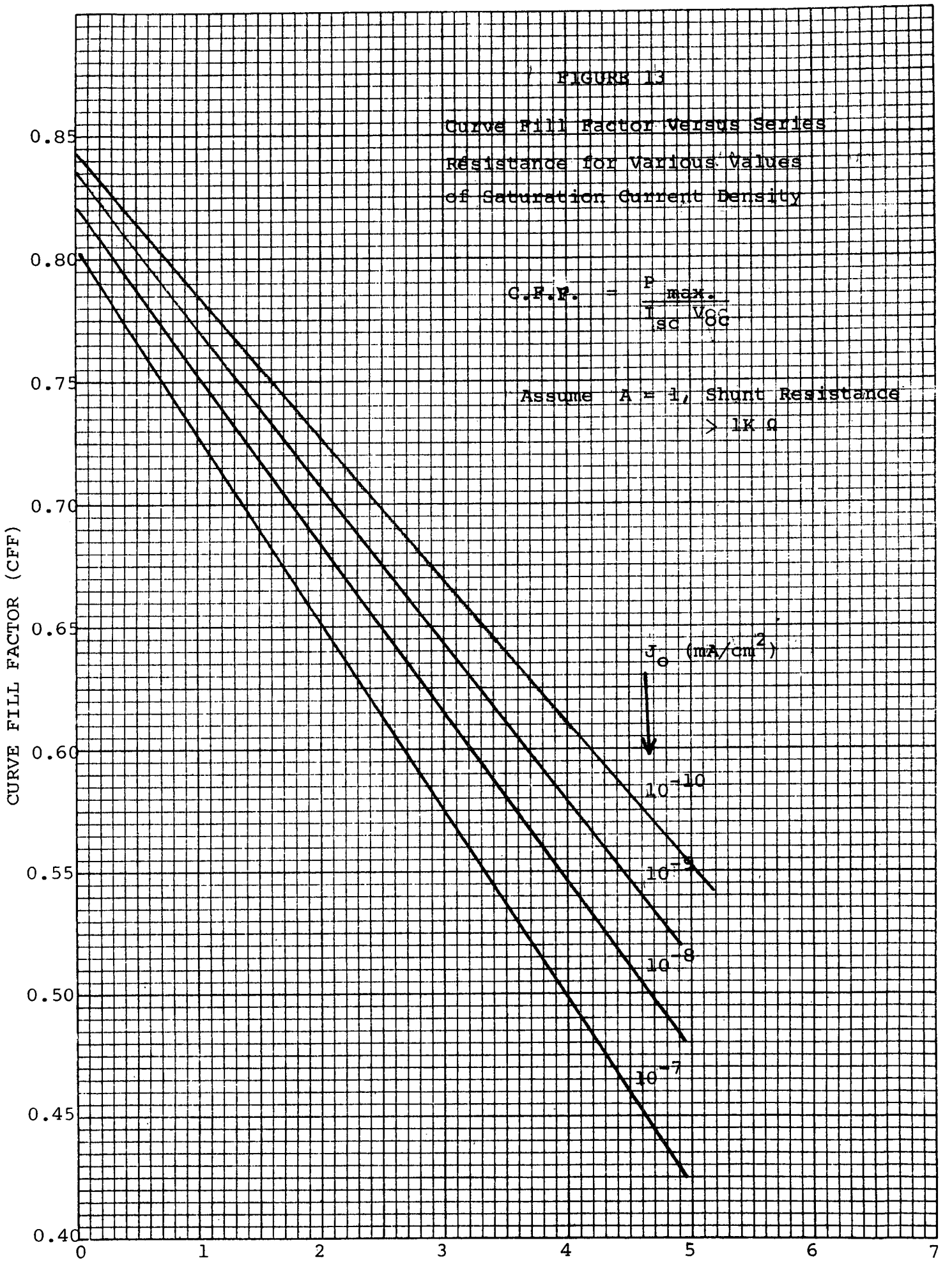

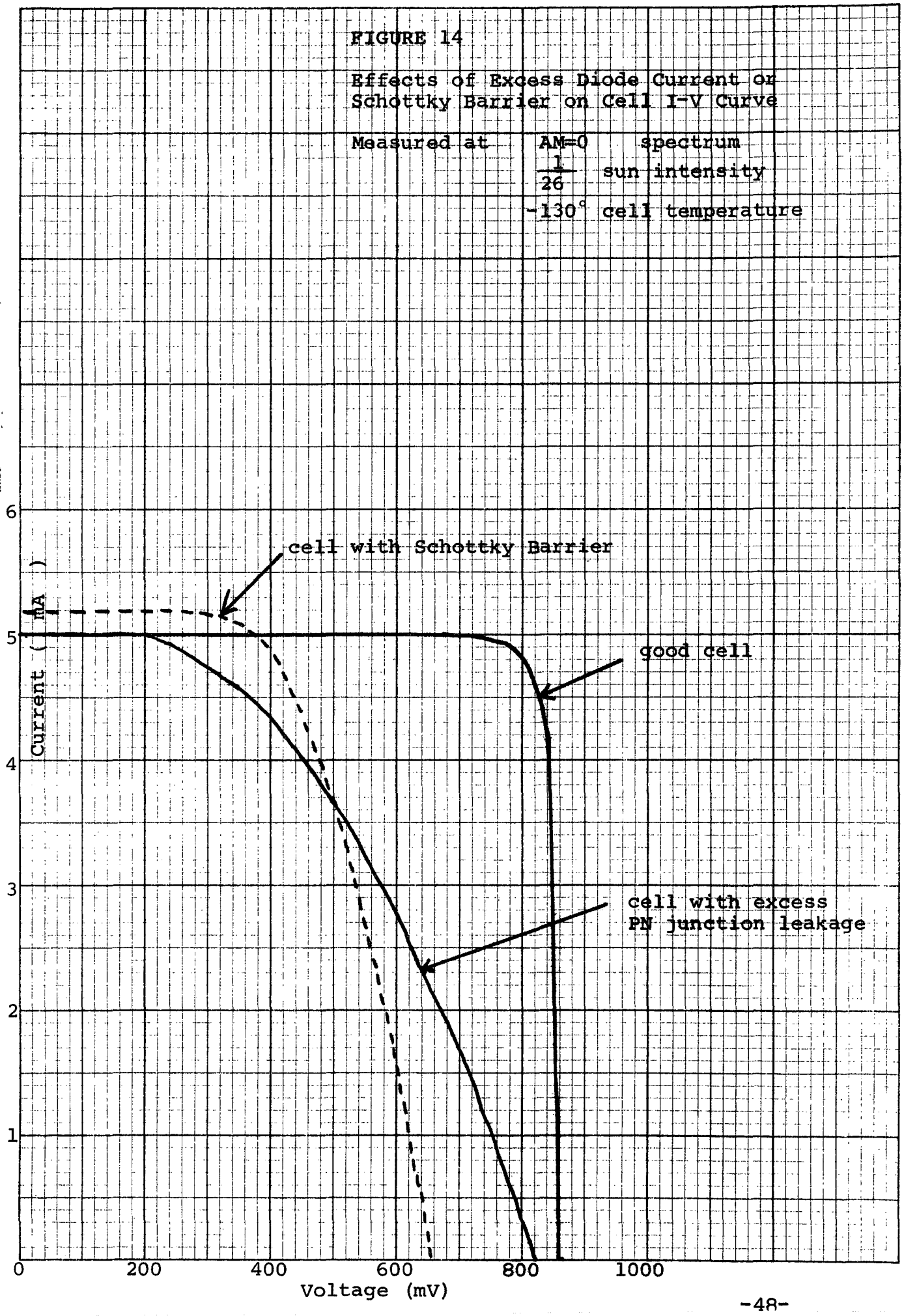
FIGURE 14
Effects of Excess Diode Current or Schottky Barrier on Cell I-V Curve
Measured at AM=0 spectrum
1/26 sun intensity
-130° cell temperature
cell with Schottky Barrier
good cell
cell with excess PN junction leakage
Current (mA)
Voltage (mV)
0
200
400
600
800
1000
1
2
3
4
5
6

In practice, additional tolerance to harmful interaction between these process steps can be gained by increasing the junction depth to around 1μm. The resultant loss of current because of reduced short wavelength response is only around 15% and this is an acceptable loss to ensure maintaining good CFF at lower temperatures.

Examination of actual cell behavior shows that present day processing can be carefully controlled to minimize these causes for excess diode current for at least 50% of the cells. It is not yet possible to prepare a specification which will guarantee sufficiently low excess current for all cells processed. Experience to date has shown that the diode excess current is less for high resistivity (10 ohm-cm) silicon.

A possible method of screening cells is available. The diode excess current can be observed in measurement of the dark-forward-biased diode characteristics at the low temperatures.

Such a measurement is considerably easier than the photovoltaic measurement at the actual mission conditions, and affords an in-process monitoring step.

Another severe decrease in CFF would result from increased series resistance resulting from carrier freeze-out. In this, the operating temperatures are not sufficient to provide thermal ionization of the impurities to give impurity conduction. Estimates showed that freeze-out effects are not expected even at Jupiter temperatures, and this prediction is confirmed by the relatively low values of series resistance obtained in cell measurements under Jupiter-like conditions. Table 12 shows approximately the temperatures at which cell performance fell off severely.

TABLE 12

Onset Temperatures for Cell Degradation

Illumination - AMO Spectrum, 5mW/cm^2 Intensity
(Onset Temperatures Underlined)

Cell Temperature (°C)	-40	-80	-120	-160
Schottky Barrier Effects				
V_{oc} (mV)				
10 ohm-cm P-Si, unsoldered	630	<u>740</u>	860	930
10 ohm-cm P-Si, soldered	620	<u>720</u>*	750*	710*
2 ohm-cm P-Si, unsoldered	650	750	<u>850</u>	950
2 ohm-cm P-Si, soldered	600	<u>720</u>*	800*	850*
Double Slope I-V				
Pmax (mW)				
10 ohm-cm P-Si, unsoldered	1.9	<u>1.9</u>	2.0	2.0
10 ohm-cm P-Si, soldered	<u>2.0</u>	1.8	1.4	1.2
2 ohm-cm P-Si, unsoldered	2.4	2.8	3.2	<u>3.6</u>
2 ohm-cm P-Si, soldered	<u>1.5</u>	1.2	<1.0	<1.0

*Indicates curves had ski-slope near V_{oc}.

The number given illustrate the trends. There was often wide variations within the groups of cells.

The unsoldered cells are seen to be better generally than soldered cells.

4.2.3.5 Cell Configuration

Most of the work described has been for N/P confuguration cells. In terms of the minimum process problems, P/N cells have given better low temperature performance. However, tests so far have shown that for the particle irradiation levels anticipated for Jupiter, N-silicon still degrades faster than P-silicon at the low mission temperatures, following the behavior seen for near-Earth missions. For the two other outer missions, P/N cells may show slight advantage over N/P cells, but it is felt that the problems outlined above can be solved for N/P cells as fully as for P/N cells, and therefore the cells designed here for all five missions under consideration will be of the N/P type.

4.2.3.6 Choice of Bulk Resistivity

In above sections, low temperature defects were often less pronounced for lower resistivity silicon, particularly the onset of a Schottky barrier which is lower for highly doped silicon. Thus, for the Mars mission a resistivity range close to that which is optimum for near-Earch (1-3 ohm-cm) is specified. For the two outer missions, a compromise is needed. It has been generally more difficult to provide P/N junctions of really low leakage with low resistivity ($\sim$1 ohm-cm) silicon. The reasons are complex, and involve the diffusion-introduced defects associated with very shallow, highly doped diffused layers. With the provision of a P+ layer under the back contact, the greatest additional cuase for cell degradation lies in the chance of severe loss of I-V curve slope. Thus, for the two lower temperature missions, it seems preferable to use slightly higher resistivity (3 to 7 ohms-cm) combined with a deeper diffusion at the expense of somewhat lower V_{oc}, but with slight advantage in radiation resistance.

4.2.3.7 Effects of Solder Coverage

There are good systems reasons to minimize the total weight of the solar cell array for the outer missions. The reasons include the large area needed to compensate for the reduced solar intensity input, and for the larger amount of antenna power needed to transmit information back to earth. These system limitations require that a minimum of solder coverage be provided on the cells because the solder adds significantly to cell weight. A method for interconnecting solderless cells can be used; e.g., welding silver interconnects to the silver contact surfaces of the cells. Alternatively, small preselected areas on the cell contacts can be solder-tinned to allow local soldered interconnects to be made.

In addition to the weight limitations, experience has shown that solder covered cells are likely to degrade faster at low temperatures than unsoldered cells, probably as a result of the thermal mismatch between the thicker solder and the silicon. An example of the harmful effects of full solder coverage can be seen by comparing the threshold temperature for onset of either the Schottky barrier described in Section 4.3.2, or of the double slope I-V curve described in Section 4.3.4.4. Table 12 gives the temperature at which degrading effects of these two phenomenon were observed.

It is preferable, then, to use no solder or minimum area solder coverage. Present day solar cells are often made with a full coverage of a thinned layer of solder (0.5 to 1.5 mils thick) but even this approach does not seem suited to low temperature missions such as the asteroid belts and Jupiter.

4.2.4 Approach Followed for Cell Optimization

The three outer missions vary in the extent of low temperature operation, and therefore in the severity of the effects described above. The Mars mission resembles near-Earth missions more closely. However, it does not add much complexity to include a P+ layer, so this layer has been provided for all three missions. On the other hand, the use of a deeper junction will give lower I_{sc} and such a junction has been specified only for the two outer missions.

The next sections give the detailed cell parameters chosen, with the above discussion in mind. Clearly, compromise decisions were often required. Again Table 1 contains a summary of the cell designs chosen.

Base Resistivity and Type

(a)	Mars	1-3 ohm-cm, boron doped
(b)	Asteroid Belts Jupiter	3-7 ohm-cm, boron doped

Junction Characteristics

(a)	Mars	20 ohms/sq. ($\sim$0.6μm), phosphorus
(b)	Asteroid Belts Jupiter	15 ohms/sq. ($\sim$1.0μm), phosphorus

Contact Materials

Mars Asteroid Belts Jupiter	Sintered titanium-silver; solderless with P+ layer formed on P-silicon.

Grid Pattern and Size

(a)	Mars	Four grids, each 2×10^{-4}m (8 mils) wide
	Asteroid Belts	Two grids, each 2×10^{-4}m (8 mils) wide
	Jupiter	One grid, each 2.5×10^{-4}m (10 mils) wide

Antireflection Coatings

Mars Asteroid Belts Jupiter	8×10^{-8}m (800Å) SiO

Handling Characteristics and Restraints

(a)	Mars	No additional constraints
(b)	Asteroid Belts Jupiter	Great care needed in preparation of front surface for P/N junction formation, and in handling of cell during subsequent fabrication, to ensure minimum junction leakage. This care must extend to controlling (and perhaps reducing) the sintering temperature-time sequence. Diode characteristics to be monitored at low temperatures.

Production Costs and Implementation Time

(a)	Mars	Very little increased cost over near-Earth cells. Need slight changes in mask used for grids.
(b)	Asteroid Belts Jupiter	Slightly increased costs in altered fabrication (deeper junction, added P+ layer) and greater care in handling throughout fabrication sequence. Need altered grid masking.

Weight

All cells will be similar in weight to conventional cells (0.35 gm. for 2x2cm cell, 0.036cm thick).

Special Tooling

Need different grid masks.

4.3 Trade-Studies of Analysis

These were mainly covered in the preceding section. They may be summarized as follows:

(a) For Mercury, the series resistance had to be reduced at the expense of reduced I_{SC} by using deeper PN junction and low resistivity silicon. Also, the cell temperature was reduced at the expense of I_{SC} by using a large fraction of reflective front contact.

(b) For Venus, low series resistance was achieved by slight reduction of I_{SC} resulting from deeper junction and low resistivity silicon.

For both (a) and (b) the V_{OC} and operating voltage of the cells was increased by the use of low resistivity silicon, which also led to lower temperature coefficients of change in I_{SC} and V_{OC}.

(c) For Mars, the Asteroid belts and Jupiter, the I_{SC} was reduced by 15% by using a depper junction to maintain good I-V curve shape at low temperature. The overall I_{SC} reduction was lower than 15% because increased active area was gained because of the need for fewer grids.

A list of the cell design parameters chosen for the various missions following this theoretical analysis was given in Table 1.

5.0 FABRICATION PHASE

The cells were fabricated using current production procedures. The silicon ingots of suitable resistivity were all grown at Centralab and were mechanically shaped (cut, sliced and polished). The N+ layers were diffused using phosphorous oxychloride gas, and the N+ layer was removed from the back surface of the cell by etching. Contacts were vacuum evaporated, using TiAg for the front contact, through a photoetched shadow mask to form the correct grid configuration. The back contact was evaporated, using TiAg or Al-TiAg as required. The contact adhesion was improved by a sintering cycle (600°C for 5 minutes in an hydrogen atmosphere). This sintering cycle led to alloying of the Al contact.

An antireflecting coating of silicon monoxide was evaporated on the front surface. The thickness of this coating was controlled to be a quarter wavelength thick near 6000A° the wavelength where the product of the cell spectral response and the AMO spectrum reaches a maximum value. The control of the SiO thickness was by means of a quartz crystal monitor. The cells were masked on the two major surfaces, and the junction edges were cleaned of leakage paths by etching. The cells were then ready for measurement.

5.1 Fabrication of Mission Design Cells

The design parameters shown in Table 1, Section 1.3 were the results of the above analysis. The fabrication sequence was adjusted to provide cells with these parameters, hopefully optimized for each mission. Table 13 shows the groups of cells with their identifying symbols and lists the physical properties of the cells. For cells intended for the Asteroid belts or Jupiter, extra care was taken in fabrication and handling. This extra care included minimum contact with the cell front surface, and reduced contact sintering cycles. Figure 15 shows grid patterns used for these Mission design cells.

5.2 Fabrication of Matrix Cells

These groups used the sixteen combinations of four pairs of variables. These variables were 0.1 or 10 ohm-cm resistivity silicon, PN junction depth 0.4 or 1.6 um, either no grids or six grids on the front contact, and with or without Al alloyed between the P-silicon and the Ti-Ag back contact. Table 14 shows the Matrix Groups, with their identifying symbols.

TABLE 13

DESCRIPTION OF MISSION DESIGN CELL GROUPS

GROUP DESIGNATION	SILICON RESISTIVITY (ohm-cm)	JUNCTION DEPTH (μm)	BACK CONTACT	GRID CONFIGURATION	TARGET MISSION
I.A	1	0.4	Ti-Ag	Checkerboard	Mercury
II.A	1	0.4	Ti-Ag	4 wide grids	Mercury
II.B	1	1.0	Ti-Ag	4 wide grids	Mercury
III.A	1	0.4	Ti-Ag	10 grids	Venus
III.B	1	1.0	Ti-Ag	10 grids	Venus
IV.A	2	0.4	Ti-Ag	6 grids	Earth
IV.B	10	0.4	Ti-Ag	6 grids	Earth
V.A	2	0.4	Al-Ti-Ag	4 grids	Mars
V.C	10	0.4	Al-Ti-Ag	4 grids	Mars
VI.B	2	1.0	Al-Ti-Ag	2 grids	Asteroid Belts
VI.D	10	1.0	Al-Ti-Ag	2 grids	Asteroid Belts
VII.B	2	1.0	Al-Ti-Ag	1 grid	Jupiter
VII.D	10	1.0	Al-Ti-Ag	1 grid	Jupiter

FIGURE 15

Grid Designs used for Various Mission Design Groups

Inner Missions

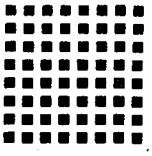

Checkerboard

6 Wide Grids

10 Grids

Earth

6 Grids

Outer Missions

4 Grids

2 Grids

1 Grid

TABLE 14

DESCRIPTION OF MATRIX CELL GROUPS

GROUP DESIGNATION	SILICON RESISTIVITY (ohm-cm)	JUNCTION DEPTH (μm)	BACK CONTACT	NUMBER OF GRIDS
1.A	0.1	0.4	Ti-Ag	6
1.B	0.1	0.4	Al-Ti-Ag	6
1.C	10	0.4	Ti-Ag	6
1.D	10	0.4	Al-Ti-Ag	6
2.A	0.1	0.4	Ti-Ag	0
2.B	0.1	0.4	Al-Ti-Ag	0
2.C	10	0.4	Ti-Ag	0
2.D	10	0.4	Al-Ti-Ag	0
3.A	0.1	1.6	Ti-Ag	6
3.B	0.1	1.6	Al-Ti-Ag	6
3.C	10	1.6	Ti-Ag	6
3.D	10	1.6	Al-Ti-Ag	6
4.A	0.1	1.6	Ti-Ag	0
4.B	0.1	1.6	Al-Ti-Ag	0
4.C	10	1.6	Ti-Ag	0
4.D	10	1.6	Al-Ti-Ag	0

5.3 Fabrication of Deliverable Cell Groups

Toward the end of the contract eight additional groups of cells were fabricated. These included five groups, each group designed for one of the five target missions. However, one additional group was included to allow further comparison of both the wide grid and checkerboard designs for Mercury cells. In addition, two more groups were added for the extreme missions.

For Mercury operation, the JPL Technical Monitor suggested the use of a spiral contact area which would reflect 60% of the incident sunlight. This contact structure is shown in Figure 16.

For Jupiter operation tests, JPL suggested a trial of higher resistivity silicon (20-30 ohm-cm) than is normally used for cells. The choice of this resistivity range stemmed in part from the analysis in the present contract which showed that better PN junction quality could be obtained from higher resistivity silicon.

The other points considered for the higher resistivity silicon were that the added series resistance from higher bulk resistivity would be less severe for the low intensity use, and also that possibly the radiation resistance of the higher resistivity cell would be increased -- an important mission requirement -- but one which was not required at the inception of this contract. The eight deliverable cell groups are described in Table 15.

FIGURE 16

Grid Designs for Mercury Mission

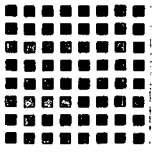

Checkerboard

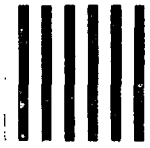

6 Wide Grids

Spiral

TABLE 15

DESCRIPTION OF DELIVERABLE CELL GROUPS

GROUP DESIGNATION	SILICON RESISTIVITY (ohm-cm)	JUNCTION DEPTH (μm)	BACK CONTACT	GRID CONFIGURATION	TARGET MISSION
#1	0.8	0.7	Ti-Ag	Checkerboard	Mercury
#2	0.8	0.7	Ti-Ag	4 wide grids	Mercury
#2S	0.8	0.7	Ti-Ag	Spiral	Mercury
#3	0.8	0.5	Ti-Ag	10 grids	Venus
#4	2.0	0.5	Al-Ti-Ag	4 grids	Mars
#5	5.0	0.7	Al-Ti-Ag	2 grids	Asteroid Belt
#6	5.0	0.7	Al-Ti-Ag	1 grid	Jupiter
#7	20.0	0.7	Al-Ti-Ag	1 grid	Jupiter
Controls	2.0	0.4	Ti-Ag	6 grids	Earth
Controls	10.0	0.4	Ti-Ag	6 grids	Earth

6.0 MEASUREMENTS

A large part of the program involved measurement of cell properties at various conditions, and analysis of these measurements. Fuller details of the test equipment and procedure are given in Appendix A.

6.1 Measurement Facilities

6.1.1 Routine Equipment

The following routine equipment was used:

(a) Solar simulators (tungsten-xenon plus filters), giving AMO spectrum 140 mW/cm^2. Cells could be maintained at 28°C ± 2% during test, and all the cells made were tested under these conditions.

(b) The forward biassed and reverse biassed I-V characteristics of the cells in the dark could be measured.

(c) On selected cells, spectral response was measured using a filter wheel.

(d) On cells typical of the various groups, PN junction depth, sheet resistance and series resistance were measured.

6.1.2 Special Equipment

Some special tests were run specifically for this program. The tests were:

(a) A performated light box which fitted under the solar simulators, providing 5 mW/cm^2.

(b) A tungsten iodide lamp giving high intensity, approximately 850 mW/cm^2.

For both (a) and (b) the cell temperature was maintained at 28°C.

(c) During the course of the program selected groups of cells were checked in the JPL measurement facility.

6.2 Summary of Measurements

The following Tables 16 and 17 summarize the measurements made on the cells.

6.2.1 Mission-Design Cell Groups

For the mission-design cell groups, Table 16 summarizes the I-V characteristics (Pmax, Isc, Voc and CFF), for three intensities (140, 5, 850 mW/cm^2), all the cells held at 28°C.

TABLE 16

SUMMARY OF I-V MEASUREMENTS at 28°C

MISSION-DESIGN CELL GROUPS

Intensity (mW/cm^2) →		140				5				850			
Group	Cell Parameters	Pmax (mW)	Isc (mA)	Voc (mV)	CFF	Pmax (mW)	Isc (mA)	Voc (mV)	CFF	Pmax (mW)	Isc (mA)	Voc (mV)	CFF
I A	2 ohm-cm $x_j \sim 0.4\mu m$ checkerboard	18	44	555	0.74	0.2	1.3	350*	-	97	215	590	0.80*
	+	14.5	43.5	550	0.60	0.1	1.3	377*	-	120.5	260	602	0.77
II A	2 ohm-cm $x_j \sim 0.4\mu m$ 6 wide grids	24	57	560	0.75	0.4	1.5	430*	-	142	306	590	0.78*
	+	18	53.8	555	0.60	0.3*	1.7	400*	-	148.5	326	610	0.74
II B	2 ohm-cm $x_j \sim 1.0\mu m$ 6 wide grids	18	45	550	0.72	0.3	1.3	400*	-	-	-	-	-
III A	2 ohm-cm $x_j \sim 0.4\mu m$ 10 grids	60	134	590	0.76	1.0	3.5	460	0.62	317	760	610	0.68
	+	57.2	131	585	0.74	1.1	4.5	470*	-	320.5	813	635	0.62
III B	2 ohm-cm $x_j \sim 1.0\mu m$ 10 grids	50	110	580	0.61	0.75	3.0	450	0.55	-	-	-	-

+ = JPL measurements
* = maximum value in each group

TABLE 16 (continued)

SUMMARY OF I-V MEASUREMENTS at 28°C

MISSION-DESIGN CELL GROUPS

Intensity (mW/cm^2) →		140				5				850			
Group	Cell Parameters	Pmax (mW)	Isc (mA)	Voc (mV)	CFF	Pmax (mW)	Isc (mA)	Voc (mV)	CFF	Pmax (mW)	Isc (mA)	Voc (mV)	CFF
IV A	2 ohm-cm $x_j \sim 0.4\mu m$ 6 grids	58	140	590	0.70	1.1	3.9	465	0.61	260	835	600	0.52
IV C	10 ohm-cm $x_j \sim 0.4\mu m$ 6 grids	56	142	550	0.72	1.0	4.0	445	0.56	160	860	555	0.34
V A	2 ohm-cm $x_j \sim 0.4\mu m$ 4 grids	59	142	590	0.70	-	3.7	425	-	-	-	-	-
V C	10 ohm-cm $x_j \sim 0.4\mu m$ 4 grids	54	148	550	0.67	1.0	3.9	435	0.59	-	-	-	-
	+	54.5	147	550	0.67	1.55	5.0	455	0.68	188.5	850	580	0.38
VI B	2 ohm-cm $x_j \sim 1.0\mu m$ 2 grids	50	120	590	0.70	0.8	3.0	455	0.60	-	-	-	-

TABLE 16 (continued)

SUMMARY OF I-V MEASUREMENTS at 28°C

MISSION-DESIGN CELL GROUPS

Intensity (mW/cm^2) →		140				5				850			
Group	Cell Parameters	Pmax (mW)	Isc (mA)	Voc (mV)	CFF	Pmax (mW)	Isc (mA)	Voc (mV)	CFF	Pmax (mW)	Isc (mA)	Vox (mV)	CFF
VI D	10 ohm-cm $x_j \sim 1.0\mu m$ 2 grids	47	120	550	0.71	0.8	3.0	435	0.62	-	-		-
	+	45	121.5	545	0.68	1.2	4.15	445	0.64	163.5	690	575	0.41
VII B	2 ohm-cm $x_j \sim 1.0\mu m$ 1 grid	42	118	585	0.61	0.9	3.2	465	0.61	-	-	-	-
VII D	10 ohm-cm $x_j \sim 1.0\mu m$ 1 grid	40	126	550	0.58	0.9	3.2	445	0.64	-	-	-	-
	+	37.2	123.5	545	0.55	1.05	4.2	445	0.56	108.5	520	570	0.36

Isc Values

For 140 and 5 mW/cm^2, the observed Isc variations can be explained by one or several of the following reasons:

(a) Variation in active area because of the grid pattern used. The extreme case of small active area is seen for the checkerboard design; in this case the active area is less than the planned 40% because of some splash-over of metal during evaporation. A larger active area than normal is seen for 4 grids and less.

(b) Variation in bulk resistivity. In general, 10 ohm-cm gives higher I_{sc}.

(c) Variation in junction depth. I_{sc} is decreased by approximately 20% when the junction depth is 1.0μm rather than 0.4μm.

Voc Values

These were generally as expected for the bulk resistivity used. However, cells with inferior characteristics often showed large decrease in V_{oc}.

CFF and Pmax

The CFF values at 140 mW/cm^2 are useful to predict the high intensity performance. For example, groups IA, IIA, show promise. However IIIA had good CFF at 140 mW/cm^2, but lower CFF at 6 suns. This shows that the 10 grid pattern alone was not sufficient to offset the reduced CFF resulting from the shallow junction.

Selection of Cells for Inner Missions Simulated Tests

For actual inner mission tests, based on overall I-V characteristics, groups IA, IIA, IIB, IIIA and IIIB will be compared to group IVA.

Selection of Cells for Outer Missions Simulated Tests

The CFF values for the groups planned for the outer missions showed that the following groups are worthy of more detailed testing. The groups to be compared with IVA are IIIA, VC, VIB, VID, VIIB, and VIID.

Dark Diode I-V Characteristics

It was hoped that for the wide variety of cell parameters involved, measurement of the dark diode characteristics might allow some information to be gained, to check the possible operation for the various missions. In general, good correlation was found, e.g., deeper PN junctions gave better reverse characteristics. However, specific correlation between the dark diode values and the various

I-V measurements at 28°C was not always obtained. Figure 17 shows the percentages within the mission-design cell groups which had designated forward or reverse characteristics. There is generally association of properties, i.e., good dark forward behavior is accompanied by good dark reverse properties.

Spectral Response

Measurements were made of the output of typical cells in the mission-design cells as ten narrow band filters were moved in front of an illuminating tungsten lamp. The ratio of the output in the ninth and second channels shows how the ratio of long wavelength to short wavelength response changes. These ratios are shown in Figure 18. The ratio is seen to increase with resistivity (because of increased long wavelength response, because of greater bulk perfection) and also with deeper junctions (because of reduced short wavelength response).

6.2.2 Matrix Cell Groups

Table 17 summarizes the matrix cell groups under the same conditions as noted in Table 16.

Isc Values

Again there is a decrease of around 10% in going from 10 to 0.1 ohm-cm resistivity. In addition, the deeper junction (1.6μm) reduces I_{sc} by an additional 20%. At 140 mW/cm^2, as expected, none of the ungridded cells show any promise.

Voc Values

Again these are as expected from the bulk resistivity, and as before, poor cells often show low V_{oc}.

CFF and Pmax

Comparison of CFF values at low or high intensity again gives a guide to groups worthy of fuller investigation.

Selection of Cells for Inner Missions Simulated Tests

The groups showing most promise for the inner missions are 3A, 3B, 3C, all incorporating deeper PN junctions and 6 grids. Cells from these groups will be compared to Group IVA in the mission design cell groups.

Selection of Cells for Outer Missions Simulated Tests

Low level readings show that the lack of grids does not prejudice low level operation seriously. The following groups had good low intensity performance, and sample cells will be compared with IVA, namely groups 1C(or 1D), 2C (or 2D), 3C(or 3D) and 4C(or 4D).

FIGURE 17

Dark Diode Characteristics for Mission Design Cells

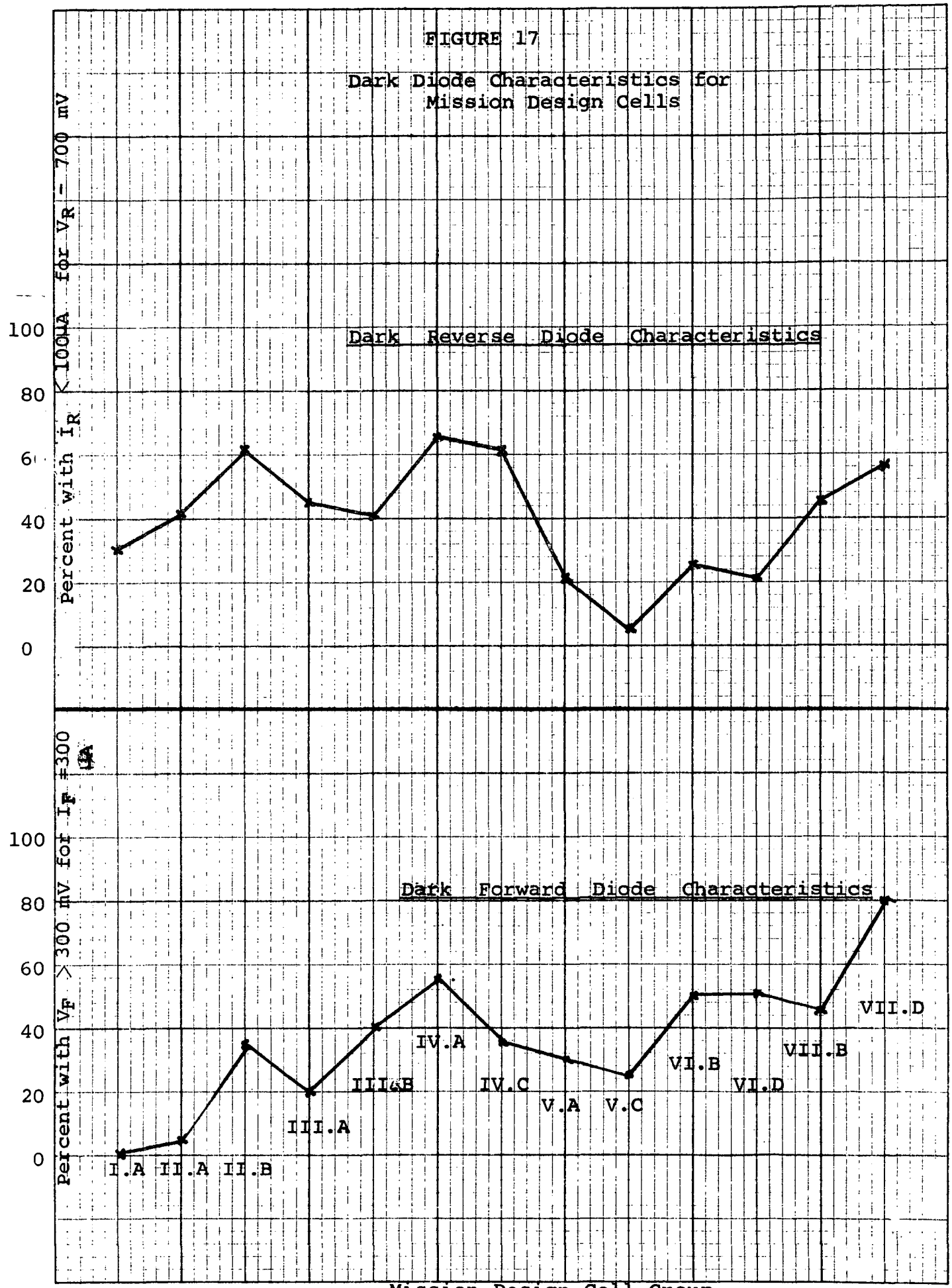

Figure 16

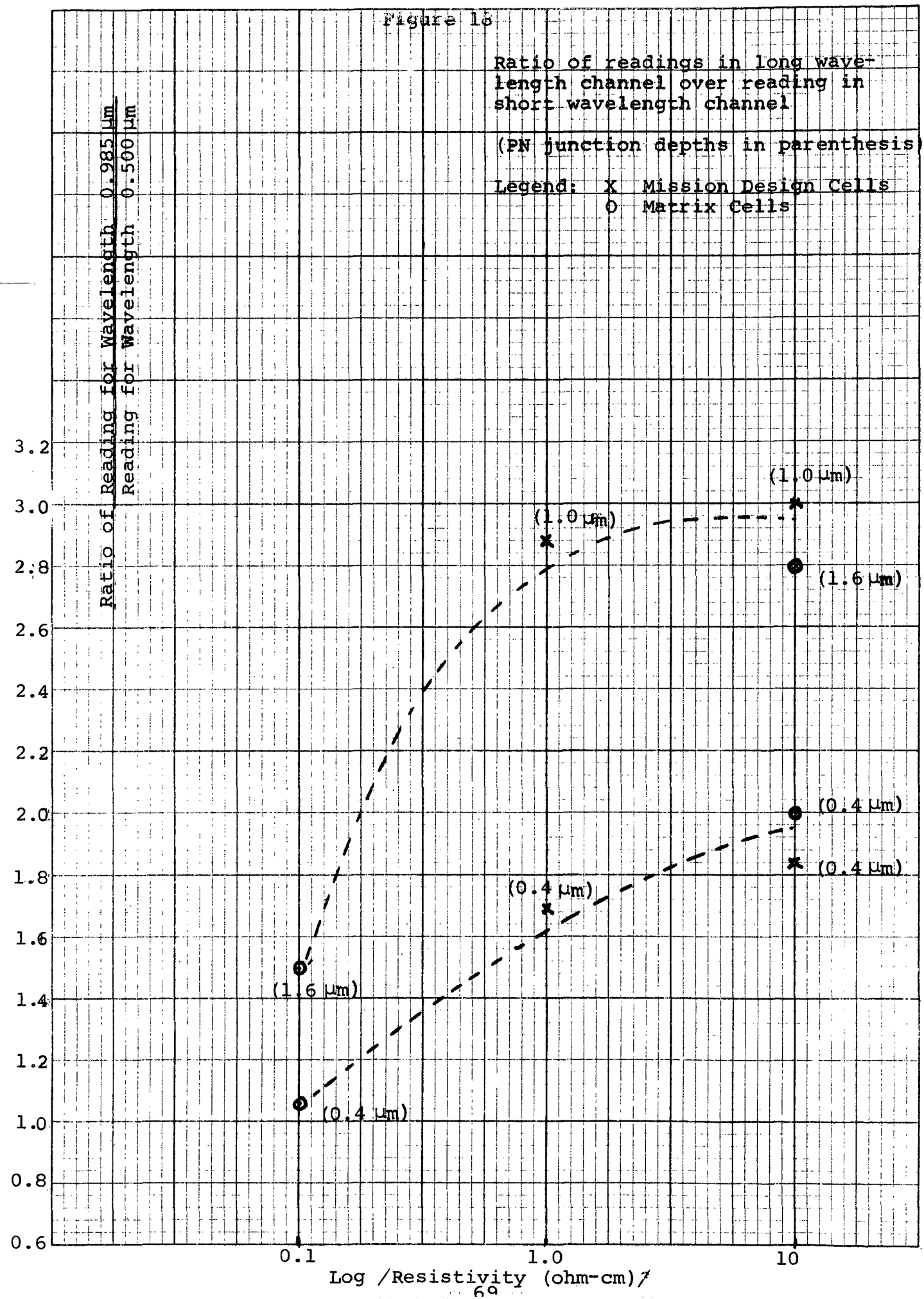
Ratio of readings in long wavelength channel over reading in short wavelength channel
(PN junction depths in parenthesis)
Legend: X Mission Design Cells
O Matrix Cells
Ratio of Reading for Wavelength 0.985 µm / Reading for Wavelength 0.500 µm
3.2
3.0
2.8
2.6
2.4
2.2
2.0
1.8
1.6
1.4
1.2
1.0
0.8
0.6
0.1
1.0
10
Log /Resistivity (ohm-cm)/
(1.0 µm)
(1.0 µm)
(1.6 µm)
(0.4 µm)
(0.4 µm)
(0.4 µm)
(1.6 µm)
(0.4 µm)

TABLE 17

SUMMARY OF I-V MEASUREMENTS at 28°C

MATRIX CELL GROUPS

Intensity (mW/cm^2) →		140				5				850			
Group	Cell Parameters	Pmax (mW)	Isc (mA)	Voc (mV)	CFF	Pmax (mW)	Isc (mA)	Voc (mV)	CFF	Pmax (mW)	Isc (mA)	Voc (mV)	CFF
1 A	0.1 ohm-cm $x_j \sim 0.4\mu m$ 6 grids Ti-Ag back	55	126	600	0.73	0.8	3.4	400*	0.59	275	520	630*	-
1 B	0.1 ohm-cm $x_j \sim 0.4\mu m$ 6 grids Al-Ti-Ag back	55	126	555	0.79	0.5	3.4	300	0.48	-	590	490*	-
1 C	10 ohm-cm $x_j \sim 0.4\mu m$ 6 grids Ti-Ag back	55	139	550	0.72	1.2	3.9	460	0.67	185*	890	570	-
1 D	10 ohm-cm $x_j \sim 0.4\mu m$ 6 grids Al-Ti-Ag back	57	140	560	0.73	1.2	3.9	460	0.67	-	850	460	-
2 A	0.1 ohm-cm $x_j \sim 0.4\mu m$ 0 grids Ti-Ag back	10	50	580	0.35	0.8	3.5	380*	0.60	19*	100	565	-

* = maximum value in each group

TABLE 17 (continued)

SUMMARY OF I-V MEASUREMENTS at 28°C

MATRIX CELL GROUPS

Intensity (mW/cm^2) →		140				5				850			
Group	Cell Parameters	Pmax (mW)	Isc (mA)	Voc (mV)	CFF	Pmax (mW)	Isc (mA)	Voc (mV)	CFF	Pmax (mW)	Isc (mA)	Voc (mV)	CFF
2 B	0.1 ohm-cm $x_j \sim 0.4\mu m$ 0 grids Al-Ti-Ag back	8	50	560	0.29	0.2	2.0	200	0.50	-	95	420	-
2 C	10 ohm-cm $x_j \sim 0.4\mu m$ 0 grids Ti-Ag back	10	50	550	0.38	1.1	4.2	460	0.57	-	100	475	-
2 D	10 ohm-cm $x_j \sim 0.4\mu m$ 0 grids Al-Ti-Ag back	10.5	50	550	0.38	1.1	4.2	360	0.57	-	85	500	-
3 A	0.1 ohm-cm $x_j \sim 1.6\mu m$ 6 grids Ti-Ag back	50	106	600	0.80	0.8	2.9	470	0.59	250	520	635	0.75
3 B	0.1 ohm-cm $x_j \sim 1.6\mu m$ 6 grids Al-Ti-Ag back	50	106	600	0.80	0.9	2.9	480	0.64	230	525	630	0.70
3 C	10 ohm-cm $x_j \sim 1.6\mu m$ 6 grids Al-Ti-Ag back	50	120	550	0.75	1.1	3.4	460	0.70	290	725	595*	0.67

TABLE 17 (continued)

SUMMARY OF I-V MEASUREMENTS at 28°C

MATRIX CELL GROUPS

Intensity (mW/cm^2) →		140				5				850			
Group	Cell Parameters	Pmax (mW)	Isc (mA)	Voc (mV)	CFF	Pmax (mW)	Isc (mA)	Voc (mV)	CFF	Pmax (mW)	Isc (mA)	Voc (mV)	CFF
3 D	10 ohm-cm $x_j \sim 1.6\mu m$ 6 grids Al-Ti-Ag back	51	120	550	0.77	1.1	3.4	460	0.70	67	770	485	0.18
4 A	0.1 ohm-cm $x_j \sim 1.6\mu m$ 0 grids Ti-Ag back	20	90	600	0.37	1.0	3.2	470	0.67	50	240	590	0.35
4 B	0.1 ohm-cm $x_j \sim 1.6\mu m$ 0 grids Al-ti-Ag back	17	84	590	0.34	0.7	3.1	400*	0.56	19	110	535*	-
4 C	10 ohm-cm $x_j \sim 1.6\mu m$ 0 grids Ti-Ag back	19	90	550	0.38	1.2	3.6	460	0.72	-	230	440*	-
4 D	10 ohm-cm $x_j \sim 1.6\mu m$ 0 grids Al-Ti-Ag back	20	90	545	0.41	1.15	3.6	460	0.69	-	240	455	-

Dark Diode I-V Characteristics

Figure 19 shows a plot for the matrix cells corresponding to Figure 17. Again the percentage of matrix cell groups which had given forward or reverse characteristics, is plotted versus the group. The same association is seen as in Figure 16.

Spectral Response

Figure 20 shows a plot corresponding to Figure 18. The same trends are seen. The values for the matrix cells are also given in Figure 18. Figure 20 shows how I_{sc} at AMO varies for both groups of cells, as the junction depth increased.

Anomalies

In the course of the work, several anomalies were investigated. These included:

(a) The occurrence of very low V_{oc} for matrix cell groups which combined low resistivity silicon and a shallow PN junction. The probable reason was identified as penetration of the very shallow junction by front contact metals during the sintering cycle.

(b) Splash-over of contact metals when evaporating through the checkerboard, 4 wide grid or 10-grid masks. This splash-over reduced the active area of the cells. The reason was lack of close contact between the cells and the contact masks, and the remedy was to add magnetic hold-down capability to the mask fixtures.

(c) Wide I_{sc} variations in some groups were traced to surface stains, occurring as a result of incomplete cleaning of the front surface during cell fabrication. This problem was not trivial because the surface stains were generally invisible until the silicon monoxide film was evaporated on the cells. The cause of the stains was subtle, involving interaction of the surface layers left on the cell from previous processing steps, and the acids (and their concentration) used to remove these layers.

The anomalies and their solutions increased the understanding of interactions between cell parameters, and also indicated where some changes in the fabrication steps can be made in future work. Wherever critical interaction is involved between specific steps, before cells are made, small scale separate tests are needed to decide on the best sequence which will minimize interaction and thus allow reliable evaluation of the effects of separate variables.

FIGURE 19

Dark Diode Characteristics for Matrix Cells

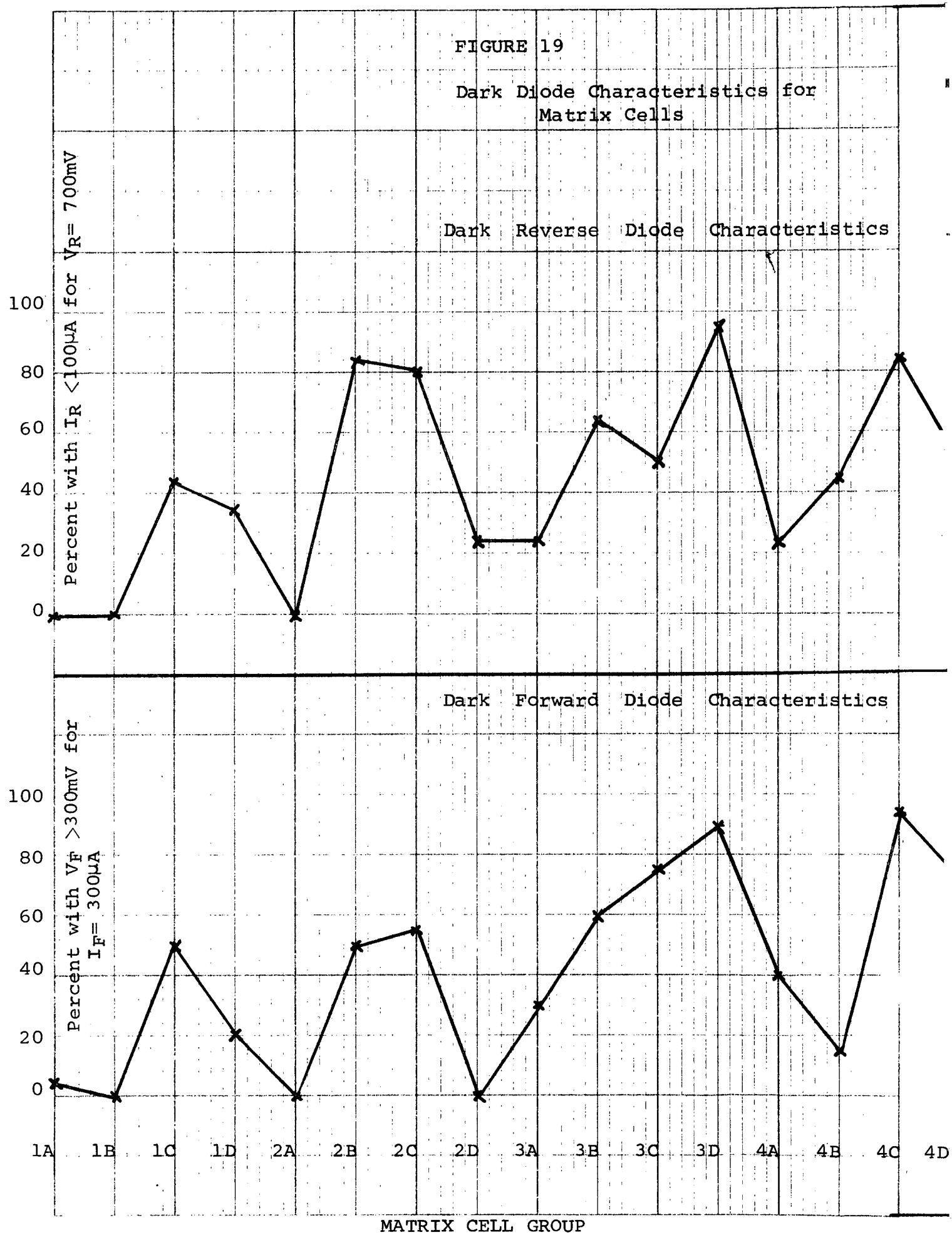

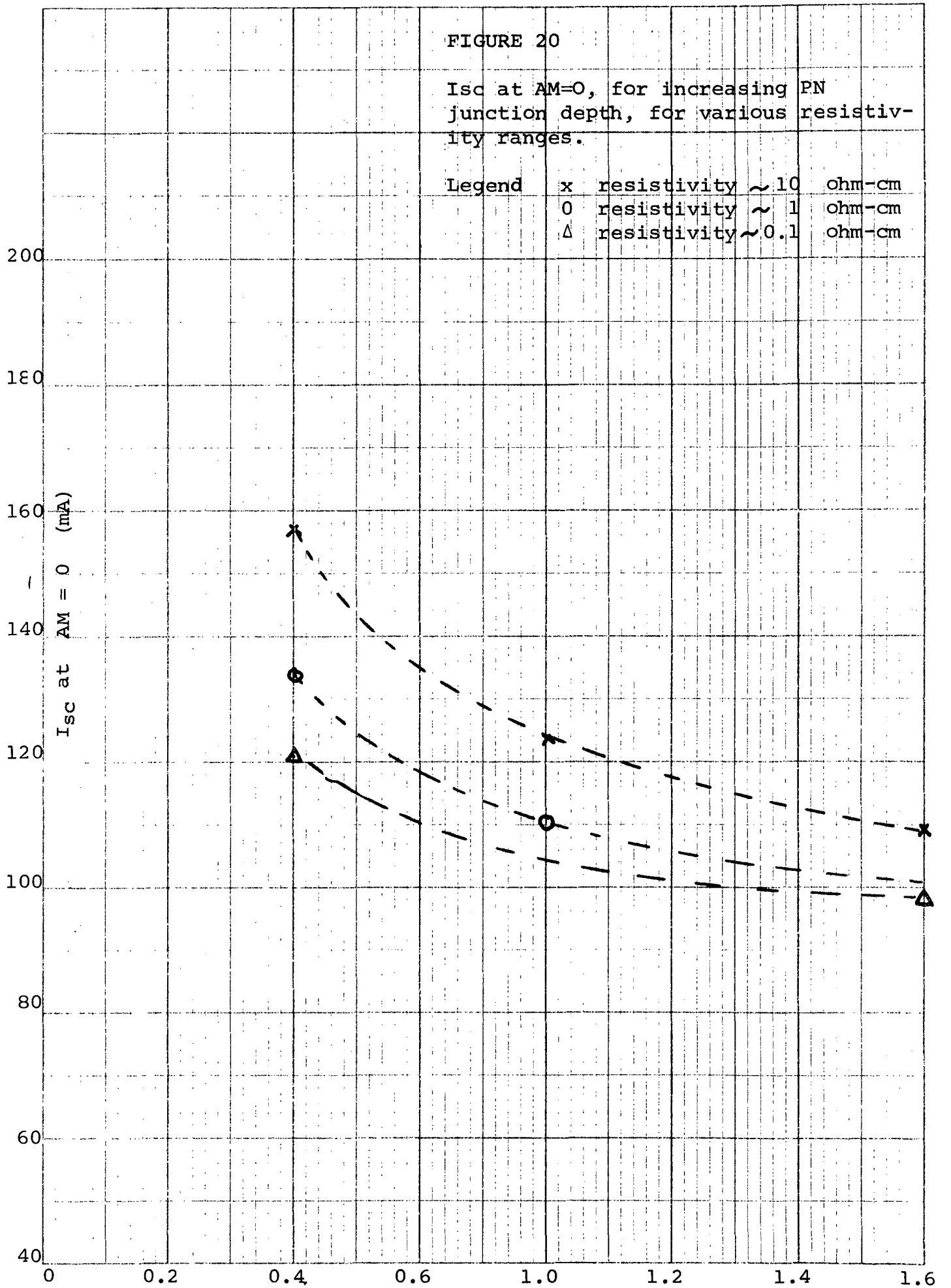
FIGURE 20
Isc at AM=O, for increasing PN junction depth, for various resistivity ranges.
Legend x resistivity ~ 10 ohm-cm
0 resistivity ~ 1 ohm-cm
Δ resistivity ~ 0.1 ohm-cm
200
180
160
140
120
100
80
60
40
I_{sc} at AM = 0 (mA)
0
0.2
0.4
0.6
1.0
1.2
1.4
1.6
PN Junction Depth (μm)

7.0 CONCLUSIONS

Because the simulated mission tests have not yet been carried out, conclusions can be made based only on the theoretical study, the cell fabrication results, and 28°C test results at three intensities covering the values at Jupiter, Earth and Mercury. Within this framework, the following conclusions can be drawn.

(1) As usual in solar cell work, it is necessary to design specifically for each mission, including all the mission requirements. For example, if tilting arrays are considered the best choice for the Mercury mission, the approach which was followed in Section 4 is too inflexible. The use of a large fraction of reflecting metal contact can limit the amount of power available for the mission as the spacecraft moves toward Mercury.

Also, although radiation goals are not defined, it is clear that these must be introduced into any program designing cells for a range of missions such as those considered here.

Also, practical factors (e.g., whether the array design can accept unsoldered cells) must be considered.

(2) With the reservations in (1), the present program has demonstrated that the present state-of-the-art can be adjusted to fabricate cells with a good chance of giving acceptable performance over the whole range considered. This is particularly true for the inner missions. Present day technology, in combinations within the range of parameters used here, is available to design cells capable of good operation for current array designs. The question of whether all the outer mission requirements can be met will depend in part on the detailed tests on cells made here, and in part on whether the overall mission needs can in fact be satisfied by solar cells.

(3) There are often interactions between the various fabrication steps and these must be known and understood, and minimized before realistic assessment can be made of the separate effects of the different cell parameters.

(4) Theoretical calculations show that there should be no advantage in shifting the minimum of the anti-reflection coating to longer wavelengths.

(5) Spectral response measurements are helpful in understanding the trends in cell properties as the parameters are changed.

(6) Unilluminated diode characteristics were not as specifically useful as expected, although general correlation was found. However, measurement of these parameters at the expected mission temperatures could allow realistic predictions of actual mission behavior, because the detailed diode properties dominate the overall cell performance, once the external properties such as light generated current, series and parallel resistance are established.

(7) The conclusions on performance in actual mission conditions will be reported separately when these tests have been run.

8.0 SUGGESTIONS FOR FUTURE CELL DESIGN WORK

As mentioned in Section 7.0, actual simulated mission tests have not yet been run for the variety of cells fabricated in this program, and therefore final suggestions cannot be made until the results of these tests are known. The results of these tests, when analyzed, should indicate some future directions to pursue.

The results to date indicate that the major area requiring further attention will be the specification of processes which ensure that the excess current in the PN junction will be low enough to provide good cells for Jupiter conditions.

It has been emphasized in this program that before mission needs can be met, consideration must be given to the total array needs, including the weight and mechanical needs, and also the radiation requirements. Some of the cells fabricated in this program will be useful for such radiation tests, and will be evaluated for their radiation resistance.

9.0 REFERENCES

1. Drummond, A. J. - Precision Radiometry and its Significance in Atmospheric and Space Physics" in Advances in Geophysics, Volume 14, Academic Press (1970).

2. Ross, R. A., Jr. - "Solar-Panel Approaches for a Venus-Mercury Flyby" presented at Space Technology and Heat Transfer Conference, Los Angeles, June 1970, ASME Paper 70-Av/Sp T-29.

3. Crossley, P. A. et al, "Review and Evaluation of Past Solar Cell Development Efforts". Final Report, NASA Contract NASW-1427, RCA, Princeton, N.J. (1968), Appendix II.

4. Olson, O. H., "Selected Ordinates for Solar Absorptivity Calculations", Appl. Opt. 2, 109 (1963).

5. Francon, M., "Modern Applications of Physical Optics", Interscience, New York (1963).

6. Hass, G. & Salzberg, C. D., "Optical Properties of Silicon Monoxide in the Wavelength Region from 0.24 to 14.0 Microns", J. Opt. Soc. Amer. 44, 181 (1954).

7. Runyan, W. R., "Silicon Semiconductor Technology", McGraw-Hill, New York (1965), p. 198.

8. Schmidt, E., "Simple Method for the Determination of Optical Constants of Absorbing Materials", Appl. Opt. 8, 1905 (1969).

9. R. A. Smith, "Semiconductors" Cambridge University Press 1959, p. 350.

10. K. L. Kennerud, "Electrical Characteristics of Silicon Solar Cells at Low Temperatures". IEEE Trans. on Aerospace and Electronic System, Vol. AES-3, No. 6, July 1967, p. 586.

11. J. D. Sandstrom, "Electrical Characteristics of Silicon Solar Cells as a Function of Cell Temperature and Solar Intensity". Proceedings IECED 1968, p. 138.

12. R. K. Yasui, L. W. Schmidt, "Performance Characteristics of Ti-Ag Contact N/P and P/N Silicon Solar Cells". Proceedings 8th Photovoltaic Specialists Conference 1970, p. 110.

13. R. J. Debs, W. R. Hanes, "Preliminary Results of Radiation Jupiter Environment Tests on Solar Cells", Proceedings 8th Photovoltaic Specialists Conference 1970, p. 158.

References (Cont'd.)

14. P. A. Payne, E. L. Ralph, "Low Temperature and Low Solar Intensity Characteristics of Silicon Solar Cells", Proceedings 8th Photovoltaic Specialists Conference 1970, p. 135.

15. J. C. Ho, F. T. C. Bartels, A. R. Kirkpatrick, "Solar Cell Low Temperature, Low Solar Intensity Operation", Proceedings 8th Photovoltaic Specialists Conference 1970, p. 150.

16. W. C. Dash, R. Newman, "Intrinsic Optical Absorption in Single Crystal Ge and Si at 77°K and 300°K", Phys. Rev. Vol. 99, p. 1151, 1955.

17. A. Shumka, "Temperature Effects on Silicon Solar Cells Short Circuit Currents", Proceedings 8th Photovoltaic Specialists Conference 1970, p. 96.

18. H. W. Brandhorst, R. E. Hart, "Spectral Response of Silicon Solar Cells at Low Temperatures", Proceedings 8th Photovoltaic Specialists Conference 1970, p. 142.

10.0 BIBLIOGRAPHY

The following papers contain information bearing directly on the present program.

1) J. D. Sandstrom "Electrical Characteristics of Silicon Solar Cells as a Function of Cell Temperature and Solar Intensity". Proceedings of the Intersociety Energy Conversion Engineering Conference 1968, page 138. At JPL, measured N/P cells with 2 ohm-cm base resistivity, with thicknesses extending from 0.01 cm (4 mils) to 0.045 cm (18 mils). Also evaluated some P/N cells with 1 ohm-cm resistivity silicon. The cell temperatures were varied from -100°C to +100°C, and the solar intensities used were 5, 25, 50, 100, 140 and 250 mW/cm^2. I_{sc}, V_{oc} and P_{max} were plotted both as a function of temperature and of intensity. The performance of these cells decreased at the extremes. At low intensity, low temperature, P_{max} did not increase as fast as V_{oc}, indicating decrease in CFF. At high intensity, high temperature, P_{max} decreased probably because of the increased effects of series resistance.

2) R. K. Yasui L. W. Schmidt, "Performance Characteristics of Ti-Ag Contact N/P and P/N Silicon Solar Cells". Proceedings of the 8th Photovoltaic Specialists' Conference, 1970,page 110.N/P&P/Ncells of 2 ohm-cm base resistivity were measured under simulated Jupiter and Venus conditions. The intensity range used was 5 to 250 mW/cm^2 and the temperature range was -140°C to + 140°C. Some mechanical contact tests were run, and showed a maximum for the contact strength around -50°C to - 100°C. P_{max} was measured for both cell types as a function of temperature and intensity. The two types were equivalent at low temperatures and intensities, but the N/P cells were 4% better above 140mW/cm^2. V_{oc} increased linearly with decreasing temperature for intensities above 25 mW/cm^2. At 5 mW/cm^2 V_{oc} increased more slowly at temperaturesbelow -50°C. The C.F.F. was plotted as a function of temperature and showed a maximum value around -30°C. For 5 mW/cm^2 CFF decreased for temperatures below -50°C.

3) J. V. Foster, A. C. Wilbur, D. C. Briggs, S. Friedlander "Silicon Solar Cells for Near-Sun Missions". Proceedings of the 6th Photovoltaic Specialists' Conference, 1967, page 117. This study divided into two parts, to investigate highly reflective coatings and selective filters for use on solar cells at 0.4 A.U., and the design of solar cells capable of good operation at 0.2 A.U.

The narrow band filters were good at 0.2 A.U., but poor at 1.0 A. U. The reflective coatings were not as good at 0.2 A. U., but had a better balance from 1 to 6 suns. The cells were designed to have low series resistance, by using thin slices of low resistivity (0.5 ohm-cm), normal diffusion, and eleven grids across the 2 cm dimension of the cell. These cells were superior to commercial cells above 5 suns' intensity.

4) P. A. Johnston "Laboratory Experiments on the Performance of Silicon Solar Cells at High Solar Intensities and Temperatures" NASA Technical Note, TND - 2733, March 1965. I-V characteristics of N/P (10 ohm-cm resistivity) were measured for high temperatures (to 167°C) and for high intensities (up to 600 mW/cm^2). Severe power reduction was observed at the higher temperatures. Measurements were made of the dependence of cell output as the angle of incidence of the illumination was varied. This led to the conclusion that the temperature of an array moving towards the sun could be reduced to maintain relatively constant power output, by gradually increasing the angle of incidence for closer approach.

5) W. Luft "Silicon Solar Cell Performance at High Intensities". IEE Transactions on Aerospace and Electronics, Vol A ES-6, No. 6, Nov. 1970, page 797. Tests were made of conventional 5 grid silicon cells (10 ohm-cm resistivity), special 13 grid silicon cells (0.5 ohm-cm resistivity) and a Gallium Arsenide cell, for illumination intensities from 70 to 2800 mW/cm^2 1 and for temperatures 30° to 150°C. The 13 grid cells showed superior performance giving good conversion efficiency up to 20 suns (2800 mW/cm^2).

6) J. D. Broder, H. E. Kautz, J. Mandelkorn, L. Schwartz, R. L. Ulman "Solar Cell Performance at High Temperatures". NASA Technical Note D 2529, Dec. 1964. N/P cells were made in conventional fashion, with base resistivity in the range 1 to 80 ohm-cm, and were tested at AMO, 140 mW/cm^2 at temperatures ranging from 25°C to 200°C. Without radiation, the 1 ohm-cm cells had most power output over the whole range. After irradiation by 1.5 X 10^{16} 1 MeV electrons per cm^2, the 10 ohm-cm cells had highest output up to 125°C the 1 ohm-cells giving most output above 150°C Some tests with Gallium Arsenide showed no advantage in power output up to 200°C.

7) R. G. Ross, Jr., R. K. Yasui, W. Jaworski, L-C Wen, E. Cleland "Measured Performance of Silicon Solar Cell Assemblies Designed for Use at High Solar Intensities". JPL Technical Memorandum 33-473, March 1971. Three methods were considered to reduce cell array temperatures for approach to 0.4 Au. These approaches were the mirror mosaic, the selective filter and the tilted array. Electrical and thermal characteristics were measured for several cell/coverglass array assemblies using these three methods. The cells used were N/P, either 2 or 10 ohm-cm, with three different grid patterns, namely normal grids, four wide grids and a large covered area with open cell area near the edges. Detailed measurements were given of the I-V characteristics of the various cell/coverglass combinations for intensities from 140 to 850 mW/cm^2, with cell temperatures between -40^oC and $+160^oC$.

8) C. A. Lewis, J.P. Kirkpatrick "Solar Cell Characteristics at High Solar Intensities and Temperatures". Proceedings of the 8th Photovoltaic Specialists' Conference, 1970, page 123. Silicon solar cells, some standard production types, others designed for high intensity use, were compared over an intensity range of 1 to 25 solar constants (140 to 3500 mW/cm^2) and a temperature range 28^oC to 200^oC. The cells specially designed performed well, with efficiences up to 2.5% for operation at the highest limits of intensity and temperature. Some tests were also made on the effects of these extreme conditions on coverglass and adhesives and on the variation of cell output with varying angle of incidence. Some Gallium Arsenide cells showed less percentage decrease at the high temperatures, but their overall output was lower than the silicon cells at all intensity levels.

9) K. L. Kennerud "Electrical Characteristics of Silicon Solar Cells at Low Temperatures". IEE Transactions on Aerospace and Electronics, Vol AES-3, No. 4., July 1967, page 586. P_{max}, V_{oc} and I_{sc} for P/N and N/P cells (1 ohm-cm resistivity) were measured from -196^oC to $+50^oC$ under AMO intensities of 58 and 268 mW/cm^2. The objective was to determine cell behavior for a Mars orbiting spacecraft. For the N/P cells, V_{oc} ceased to increase around -80^oC. For the P/N cells, V_{oc} increased linearly down to -196^oC. Speculation is made that the anomalous behavior of N/P cells arises from recombination center or surface leakage currents. [In retrospect it is possible that the observed anomalies could be explained by the formation of a Schottky barrier.]

10) H. Liebert "Solar Cell Performance at Jupiter Temperature and Solar Intensity" Proceedings of the 7th Photovoltaic Specialists' Conference, 1968, page 92. N/P silicon solar cells (10 ohm-cm resistivity) and cadimum sulfide cells were tested at Jupiter conditions (6 mW/cm^2, -133°C). The silicon cells varied widely, with efficiencies at Jupiter conditions varying from zero to 15%.

11) R. J. Lambert "Characteristics of Solar Cells at Low Temperatures" Proceedings of the 7th Photovoltaic Specialists' Conference, 1968, page 97. P/N silicon cells (1 ohm-cm resistivity) and N/P silicon cells (1 and 10 ohm-cm resistivity) were measured from -190°C to 27°C, at light intensities from 1 to 140 mW/cm^2. Cell efficiency at 140 mW/cm^2 and -190°C reached 16%. At -190°C the cells showed signs of constant V_{oc} as the intensity was varied. For some cells, V_{oc} increased linearly with decreasing temperature, for other cells V_{oc} reached saturation, showing signs of Schottky barrier formation.

12) W. Luft "Silicon Solar Cells at Low Temperatures" IEE Transactions on Aerospace and Electronics Systems,Vol AES-7 No. 2, March 1971, page 332. [This paper also appeared in the Proceedings of the 8th Photovoltaic Specialists' Conference, 1970, page 161]. N/P cells were measured over a temperature range of 28°C to -175°C with illumination intensities ranging from 140 mW/cm^2 to 1.5 mW/cm^2. The cells used silicon of 2 or 10 ohm-cm, and were either unsoldered, partly soldered or fully soldered. Three major anomalies in the I-V curves were noted at the low values of intensity and temperature. These anomalies were a non-horizontal curve near I_{sc} (low shunt resistance), low Voc (caused by Schottky barrier formation) and a double break (flat) near P_{max}. The measurements showed variation at the low levels in cell groups which had similar performance at 140 mW/cm^2, 28°C. Between 1/10 and 2/5 of the cell groups showed good performance at low levels (5 mW/cm^2, -120°C). The remainder of the cells showed some anomalous behavior. Only the low shunt resistance cells could be identified at room temperature. The other two anomalies only became serious at the low temperatures, and then good cells could be selected only by actual measurement at low temperatures.

The following papers all appear in the Proceedings of the 8th Photovoltaic Specialists Conference, 1970 on the pages shown.

13) Page 96 A. Shumka "Temperature Effects on Silicon Solar Cell Short Circuit Current" A theoretical analysis of the possible variation of I_{sc} with temperature. Three separate causes of variation are analysed, the changes in band gap, the variation in photon absorption coefficient, and the changes in diffusion length. These three variations are combined to calculate the change of I_{sc} with temperature. Good agreement with measured values is obtained.

14) Page 135 P.A. Payne. E.L. Ralph "Low Temperature and Low Solar Intensity Characteristics of Silicon Solar Cells" Discussed the design of cells for Jupiter conditions ($5mW/cm^2$, -135^oC). The Schottky barrier problem was eliminated by a P+ layer immediately under the back contact. The flat knee was less severe for deeper junction depth and maybe associated with the metal bar contact. Some non-linear behavior of I_{sc} versus temperature was observed for crucible grown silicon, not for oxygen-lean silicon. The efficiency under Jupiter conditions could exceed 17%.

15) Page 142 H. W. Brandhorst, Jr., R. E. Hart, Jr. "Spectral Response of Silcion Solar Cells at Low Temperatures" Spectral response of silicon cells was measured down to -180^oC. There was a general loss of red response with decreasing temperature caused by increase of the band gap leading to decreased absorption coefficient. A Schottky barrier in the back cell surface caused some loss in red response. Cells with "flat knee" had additional severe loss of red response, thought to be caused by decrease in diffusion length.

16) Page 150 J. C. Ho, F.T.C. Bartels, A.R. Kirkpatrick "Solar Cell Low Temperature, Low Solar Intensity Operation" Also deals with design of cells for Jupiter conditions. Again separates three anomalies, Schottky barrier, soft CFF (shunt leakage) and double slope in I-V curve (flat knee). In addition to photovoltaic I-V curves, use was made of the non-illuminated forward I-V characteristic at low temperatures.
All three anomalies had marked differences in this dark forward characteristic. The conclusion was that the Schottky barrier and shunt leakage problems can be solved with relatively straight forward methods, but that the flat knee is caused by excessive edge leakage and edge channelling should be avoided (ideally) by the use of a planar N/P cell

with P+ guard ring, combined with lower resistivity and possibly permanent passivation of the surfaces.

17) Page 155 R.J.Debs, N.R. Hanes "Preliminary Results of Radiation and Jupiter Enviroment Tests on Solar Cells" The Schottky barrier and double slope defects were described. They could be found from measurement of the dark forward characteristic at low temperature. A possible screening method to choose good Jupiter cells would measure the dark current at 600 mV at approximately -130^{o}C. Preliminary results are given for radiation effects at these low temperatures.

18) Page 353 R. Gereth, H. Fischer, E. Link, S. Mattes, W. Pschunder "Silicon Solar Cell Technology of the Seventies" Combines several areas of advanced cell technology. In particular discusses cells for operation at low temperatures. For high intensity (140 mW/cm^{2}) and low temperature, only the Schottky barrier amomaly was observed and was solved by use of a P+ layer under the back contact. No discussion was given of any flat I-V characteristics.

APPENDIX A

SPECIAL TEST CONDITIONS

The measurements required for this program were discussed in Section 6.1 above.

The Centralab Tungsten-Xenon Simulators are well proven for use at AMO, 140 mW/cm^2. Their calibration is based on a combination of Table Mountain measurements, and the use of JPL Ballon Flight Standard cells.

Low Intensity Measurements

By using neutral density filters, these simulators can provide the correct spectrum for the outer missions out to Jupiter. As mentioned in 6.12, a perforated screen formed the top surface of a box covering the cell-holding fixture. The screen was perforated to give 1/28 intensity reduction. The perforations provided 16 overlapping images per square inch, which gave adequate uniformity at the test plane.

There are difficulties in providing the correct cell temperature for these low intensity measurements. The usual way this has been carried out at Centralab is to solder each cell to a tinned silicon block to avoid thermal expansion problems. The blocks are mounted on a circular ring which can be moved under a window in line with the light source. The individual cell I-V characteristic can be measured by switching to wires soldered to each cell. The base to which the cells are soldered is cooled to liquid nitrogen temperature and measurements made. The base is then warmed by a heater system and by balancing the heat input, dwell-temperatures between $-190^{\circ}C$ and $28^{\circ}C$ are obtainable. There is a problem of fogging of the window between the cells and the light. This is reduced by filling the space under the window with dry nitrogen.

High Intensity Measurements

The Centralab simulators do not provide collimated light and it is therefore difficult to increase the intensity on the cells by closer approach to the simulator light sources. Therefore, an additional light source was used for light intensity measurements (up to 850 mW/cm^2). The light source used was a Tungsten Iodide Lamp, G. E. Quartz line Type # Q1000 PAR 64 NSP, with special absorption filtering which gave a spectral distribution shown in Figure 1. The Tungsten Iodide is identified by the CLASS curve. The distribution shown was measured on a Perkin-Elmer quartz prism monochromator. The curve shows that the filtering has shifted the

peak of the spectral irradiance to 0.70 μm, and has significantly suppressed the infra-red output. The anomalies in the curve near 0.85 μm are due to absorption in the first surface aluminum mirrors. The slight depression around 0.55 μm is caused by absorption by the iodine vapor in the lamp.

For comparison, Johnson's AMO curve is shown also in Figure 1.

Effect of Source Spectrum on Cell Output

Because the spectrum shown differs from AMO, it is not possible to use this source to provide accurate estimates of cell output at the higher intensities, particularly since the spectral response of the cellsdesigned for near-sun missions differs from that of the standard cells used to set the intensities. However, it is felt that the light tower being constructed can be used to scan through the cell matrix to select groups with good performance at high intensities. This source can show the relative values of curve fill factor and open circuit voltage. Estimates of the short circuit current can be made by multiplication of the typical spectral response of the cells under test and the AMO spectrum, corrected to the intensity of interest. In addition, periodic correlation will be made using the JPL concentrated AMO source.

In order to justify the use of the Tungsten Iodide System for testing at high intensities an experiment was performed to determine the effects of spectral response variability among solar cells. It is possible that even though the two illumination spectra differ widely, they may do so in regions where the cells do not have high response.

Two cells with different spectral response were taken. One cell had a spectral response typical of cells optimized for near-earth conditions, the other cell was of low resistivity silicon, and deep junction depth, designed for Mercury conditions. The cell responses (shown as curves 2A or 2B, 3A or 3B in Figure 2) were each multiplied by either of the two spectral curves in Figure 1(shown here as curves 1A, 1B). Again the tungsten iodide curve 1A is identified by the term CLASS. The resulting products are given in curves 4A, 4B, 5A and 5B. Curves 4A and 4B were scaled to have equal areas, by setting the source levels such that a conventional cell has identical I_{sc} in the two columns (in this case 69.4 mA). If the Mercury-type cell was measured under these same settings, the I_{sc} values were 55.2 mA under tungsten iodide and 53.5 mA under Johnson's curve.

The net difference is 3.2%, sufficient for selection of good cells if not for accurate specification.

Evaluation of the illuminated area at the test plane, for the tungsten iodide lamp showed a polarizing effect because of the line construction of the light source. To counteract this a diffusing screen was formed from an abraded plexiglass sheet. The resultant illumination was considered satisfactory for scanning through the various cell groups to select cells worthy of more detailed measurement.

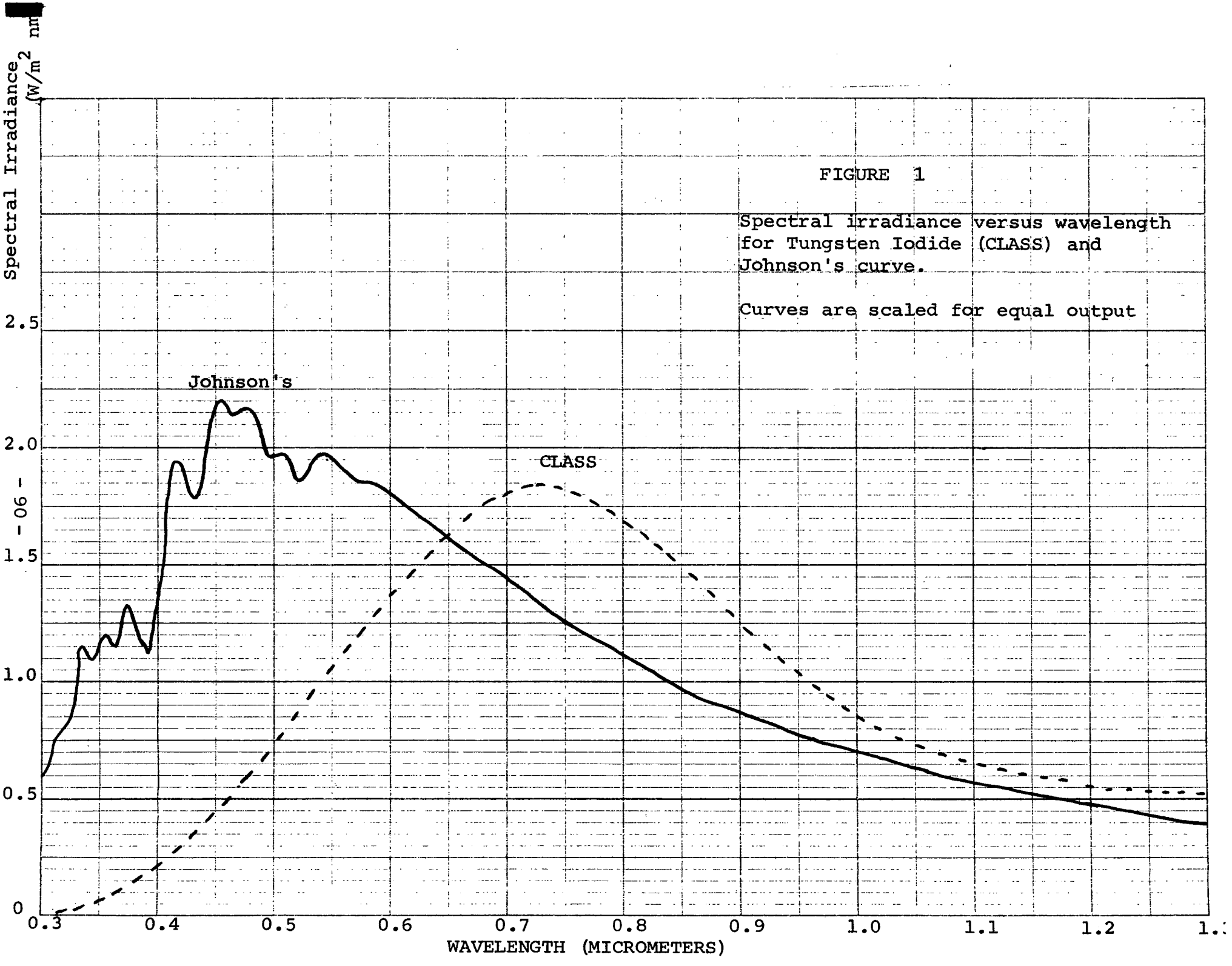

FIGURE 1

Spectral irradiance versus wavelength for Tungsten Iodide (CLASS) and Johnson's curve.

Curves are scaled for equal output

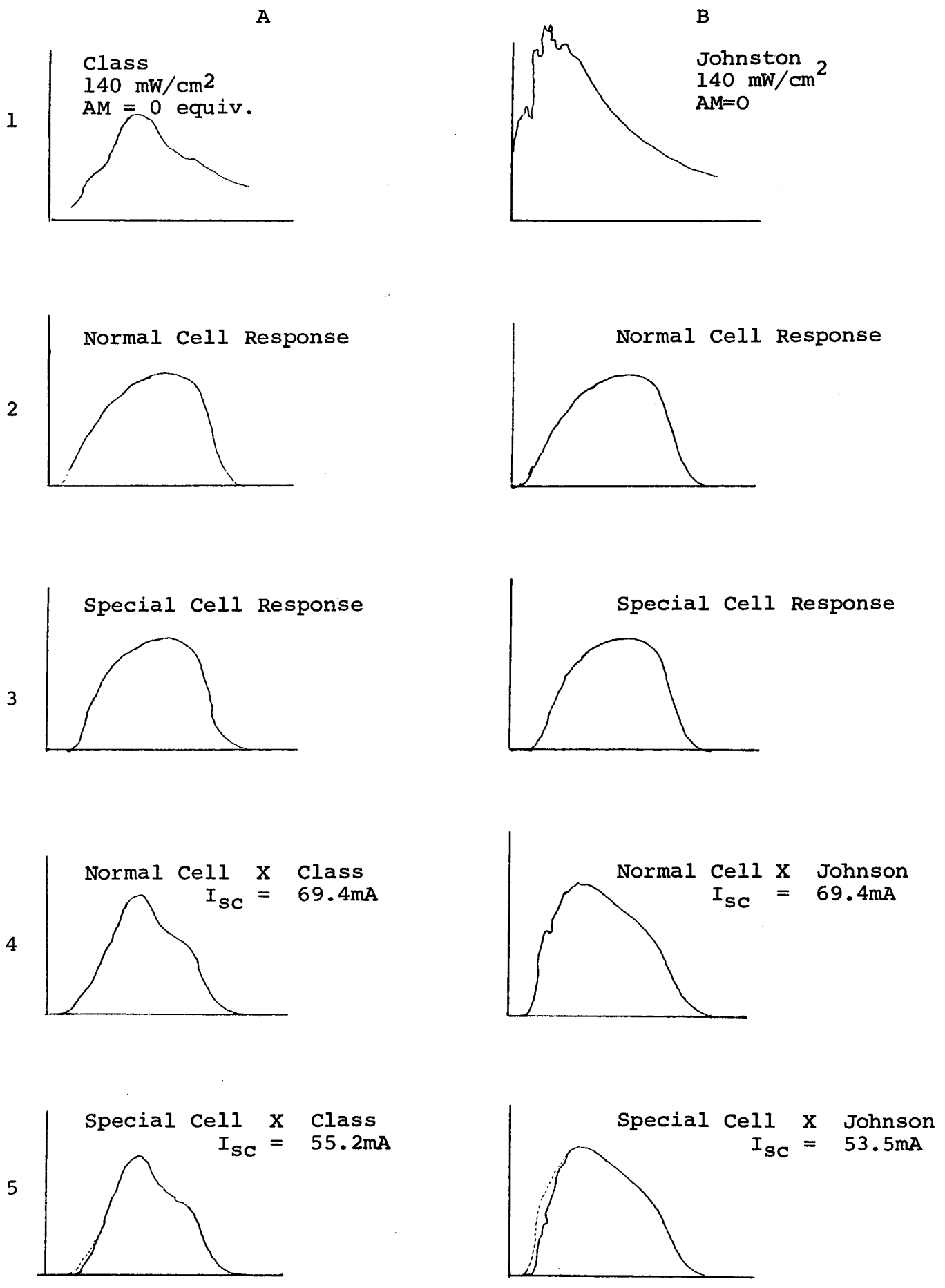

Figure 2 - Spectral Output and Spectral Response, and Products for Two Illumination Sources, and Two Cell Designs